Tuning the selectivity of the CO_2 reduction reaction by addition of zinc to a copper electrocatalyst

Lisanne M. Blom
5974550

Masterthesis

27 Oktober 2023

Debye Institute for Nanomaterials Science
Materials Chemistry and Catalysis group

Supervised by: MSc. Matt Peerlings
Examiners: Dr. Peter Ngene and prof. dr. Petra de Jongh

0. Abstract

In order to overcome both the problem of emission of greenhouse gasses and the problem of the depletion of our energy source, alternative energy sources have been investigated. Since CO_2 is the most prominent greenhouse gas and an abundant carbon source, the electrochemical CO_2 reduction reaction (eCO_2RR), to hydrocarbons and alcohols (C_{2+} products) would be a step forwards in closing the carbon cycle. In this research, copper is used as an electrocatalyst, since it is the only metal that can make C_{2+} products in significant amounts. However, the selectivity is still a big problem. Zinc is a great candidate as a promoter to improve the selectivity of the copper catalyst, due to its selective CO production, the main intermediate in the CO_2RR. The potential synergistic effects of a bimetallic copper zinc catalyst make this electrode an interesting candidate to tune the selectivity of the CO_2RR. Two different combinations of copper with zinc were used in this research: galvanic replaced and oxide-derived electrodes. The galvanic replaced electrodes showed an optimum in partial current density of CO when 2.9 - 6.2 atomic% of copper was present. This optimum is most likely caused by a promoting and a deteriorating effect counteracting. An increase in electrochemical surface area is suggested as the promoting effect and the deteriorating effect is likely due to the addition of copper in the Zn/Cu epsilon phase. The addition of ZnO nanorods to Cu_2O nanocubes in oxide-derived catalysts causes an increased activity compared to the monometallic electrodes. Unfortunately, reproducibility proves difficult and the stability of the catalysts remains a challenge, observing dissolution of zinc and dendrite formation of the copper particles during catalysis. However, the addition of zinc to the copper electrode resulted in a shift from ethylene to ethanol formation in the CO_2RR. Thus, the product formation of the CO_2RR can be tuned by changing the ratio of copper and zinc in an electrocatalyst.

Abstract for laymen

The emission of CO_2 is a big problem for the environment, since CO_2 is a greenhouse gas and therefore causes climate change. To reduce CO_2 and overcome the problem of the depletion of fossil fuels, the conversion of CO_2 towards chemicals and fuels has been greatly investigated. A promising method for this conversion is with the use of electricity in a reaction called the electrochemical CO_2 reduction reaction (eCO_2RR) In this reaction hydrocarbons and alcohols (C_{2+} products) are made, which are valuable products if we want to close the carbon cycle. Copper is the only metal that can make C_{2+} products in significant amounts. However, it forms a lot of different products, so besides our wanted C_{2+} products, multiple side products are observed. To overcome this problem, an additional metal can be introduced. Zinc is a great candidate, since it reacts CO_2 to CO, whereafter copper can use the CO to make C_{2+} products. In this research, copper and zinc are combined in different ratios via two different methods to tune the product formation of the CO_2RR. In the first method an increase in CO formation was observed when 2.9 - 6.2 atomic% of copper was present, but no C_{2+} products were formed. When less than 2.9 or more than 6.2 atomic% copper was used, the CO formation lowered. In the second method the performance in the CO_2 reduction reaction was increased. But unfortunately, the reproducibility proved difficult and the zinc copper particles were not stable. However, we did form ethylene and ethanol (both C_{2+} products) in different amounts. The addition of zinc to the copper electrode resulted in a shift from ethylene to ethanol formation in the CO_2RR. Thus, the product formation of the CO_2RR can be tuned by changing the ratio of copper and zinc in our reaction.

Table of contents

0. Abstract ---- 2
Abstract for laymen ---- 2
Table of contents ---- 3
1. Introduction ---- 5
2. Theory ---- 7
2.1. The electrochemical CO_2 Reduction Reaction ---- 7
2.2. Selectivity problem ---- 7
2.2.1. Bimetallic copper systems ---- 9
Cu/Zn bimetallic systems ---- 10
Alloys ---- 10
2.2.2. Oxide-derived electrodes ---- 11
2.2.3. Morphology ---- 12
3. Methods ---- 13
3.1 Chemicals ---- 13
3.2. Galvanic Replacement ---- 13
3.3. Oxide-derived Cu2O-ZnO-based electrodes ---- 14
ZnO nanorod synthesis ---- 14
Cu_2O nanocubes synthesis ---- 14
Working electrode preparation ---- 14
Washing treatment ---- 14
3.4 Characterization ---- 15
Scanning Electron Microscopy ---- 15
X-Ray Diffraction ---- 15
Ion Coupled Plasma ---- 15
3.5 Electrochemical measurements ---- 15
4. Results ---- 17
4.1. Galvanic replacement ---- 17
4.1.1. Catalyst characterization ---- 17
SEM-EDX ---- 17
XRD ---- 18
4.1.2. Activity ---- 19
4.1.3. Selectivity ---- 20
4.1.4. Stability ---- 21
XRD ---- 21

SEM-EDX ---- 22
4.1.5. Effect of surface roughness ---- 23
4.1.6. Discussion of galvanic replacement ---- 23
4.2. Oxide-derived Cu_2O-ZnO-based electrodes ---- 24
4.2.1. Catalyst characterization ---- 24
SEM-EDX ---- 24
X-Ray Diffraction ---- 25
4.2.2. Activity ---- 26
4.2.3. Selectivity ---- 27
Shift from ethylene to ethanol formation ---- 29
4.2.4. Stability ---- 30
SEM-EDX ---- 30
X-Ray Diffraction ---- 31
4.2.5. ICP results ---- 32
4.2.6. Discussion/Summary drop casting ---- 32
5. Conclusions and Outlook ---- 33
5.1. Conclusions ---- 33
Galvanic replacement ---- 33
Oxide derived particles ---- 33
5.2. Outlook ---- 34
6. Acknowledgements ---- 35
7. References ---- 36
8. Appendix ---- 38

1. Introduction

In the last era, wealth has taken a leap in the western world, with electricity being available to everyone and the amount of passenger cars per household still increasing. With this increase in wealth, the uptake in energy consumption has skyrocketed, see figure 1. The amount of coal, oil and gas being burnt is at an all-time high and is still enlarging.[1] With the combustion of these fossil fuels, a big problem for the environment is created: the emission of greenhouse gases.[2] Greenhouse gases heat the planet, which in turn causes rising sea levels, extreme weather and changes to plant and animal life. Furthermore, fossil fuels are depleting, making it a limited and temporary energy source.

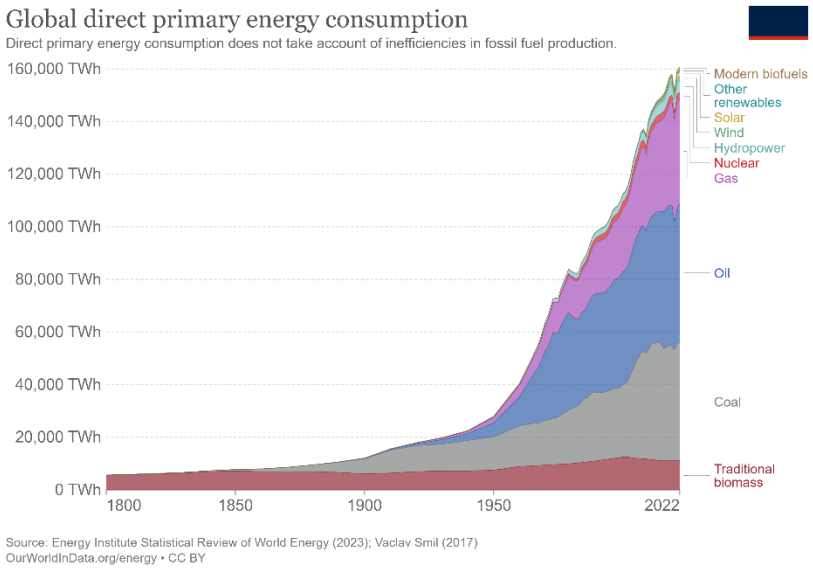

Figure 1. *The worldwide energy consumption over time separated in colour for the different energy sources. Duplicated from Our World in Data* [1]

In order to overcome both the problem of emission of greenhouse gasses and the problem of the depletion of our energy source, alternative energy sources have been investigated.[3] Renewable energy sources, such as solar energy systems, use of biomass, geothermal energy and wind energy are promising, however, they do have downsides. The biggest downside being the intermittence and fixed location of the energy source, making it difficult to get an even distribution.[4] Therefore research into energy storage and energy conversion are crucial. However, the capacity of storage and public affirmation linger. An alternative for the storage of renewable energy is the storage of emitted CO_2 with subsequential conversion into useful chemicals or fuels.[5]

Since CO_2 is the most prominent greenhouse gas and an abundant carbon source, the reduction of this molecule into hydrocarbons and alcohols (C_{2+} products) would be a step forward in closing the carbon cycle, see figure 2. A highly investigated method for this conversion is the electrochemical CO_2 reduction reaction (eCO_2RR), since it can be carried out in an electrochemical cell that operates at room temperature and in aqueous solution.[6,7] Hence, this is a sustainable reaction in case renewable electricity is used.

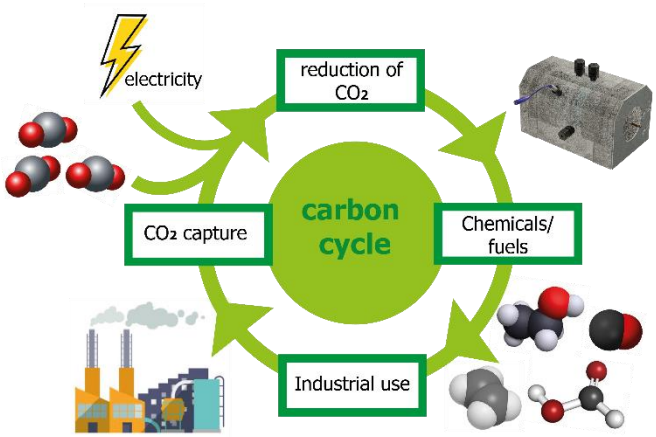

Figure 2. *A schematic representation of the carbon cycle where CO2 is reduced electrochemically. Reproduced from Albo et al.*[8]

Different reaction products can be formed in the CO_2RR, with the type of products formed depending on the binding energy of the metal catalyst used, see theory section 2.2. For example, CO is produced by Zn, Ag and Au, whereas HCOOH is produced by Pb, Sn and Bi. Some metals are inactive for CO_2RR and produce only H_2 in the competing hydrogen evolution reaction (HER). Copper is especially interesting, because it is the only metal capable of producing significant amounts of valuable hydrocarbon and alcohol products (C_{2+} products) like ethylene and ethanol.[9]

However, the selectivity towards these C_{2+} products is insufficient, with less valuable products such as CO and methane being formed.[10] Moreover, the reduction potential of the hydrogen evolution reaction is close to the reduction potential of the wanted products, producing hydrogen as an undesired side product. A last challenge in this reaction is the high overpotentials that are needed to drive this reaction in order to break the high bond energies of the CO_2 molecule. Therefore, numerous efforts have been made to improve the selectivity, stability and activity of copper-based electrocatalysts. Common strategies include the use of oxide-derived copper[11–13], tuning the morphology[14,15] and adding a second metal to create a bimetallic system[16,17]. In theory section 2.2, the specifics of these modifications to the copper electrodes will be discussed further.

The addition of zinc to a copper catalyst is promising in showing the CO spillover effect in the CO_2RR, see figure 3, making it an interesting candidate for a more selective, stable and active catalyst. We will explore the common strategies of tuning the oxidation state, morphology and chemical composition for their relevance to improving the CO_2RR performance of bimetallic CuZn-based electrodes. In this research the goal is to answer the following question: "Can we tune the CO_2RR selectivity of CuZn-based electrodes by changing their atomic composition, morphology, and oxidation state?" This will be accomplished by synthesizing different Cu-Zn electrodes and studying their catalytic activity.

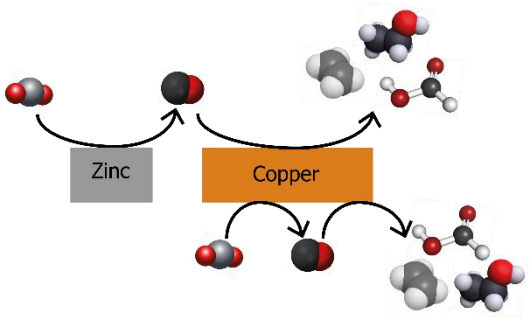

Figure 3. *A schematic representation of the CO spillover effect between zinc and copper in the CO_2 reduction reaction.*

2. Theory

This chapter describes the theory needed to correctly interpret the research executed in this thesis. Firstly, we will give background information about the general electrochemical reduction of CO_2. Then, bimetallic systems, and more specifically Zn/Cu bimetallic systems, will be discussed. Lastly, the background theory on oxide-derived electrocatalysts and morphology effects in the CO_2RR will be described.

2.1. The electrochemical CO_2 Reduction Reaction

The CO_2 Reduction Reaction (CO_2RR) is performed in an electrochemical cell. Multiple types of electrochemical cells can be used to perform this reaction. Examples are the H-cell, most commonly used to screen electrocatalysts for fundamental research,[18] the flow cell, used for representations of scale ups, and the membrane electrode assembly,[19] where the catalyst is coated directly on the membrane. In this research, an H-cell is used, as shown in figure 4. This electrochemical cell consists of an anodic and a cathodic side, separated by a membrane. On the anodic side, there is a counter electrode e.g. platinum or glassy carbon, and an anolyte. On the cathodic side, we can find the working electrode, Ag/AgCl reference electrode and a catholyte. The membrane is an anion exchange membrane, enabling anions to pass through, while keeping neutral species and cations separated.

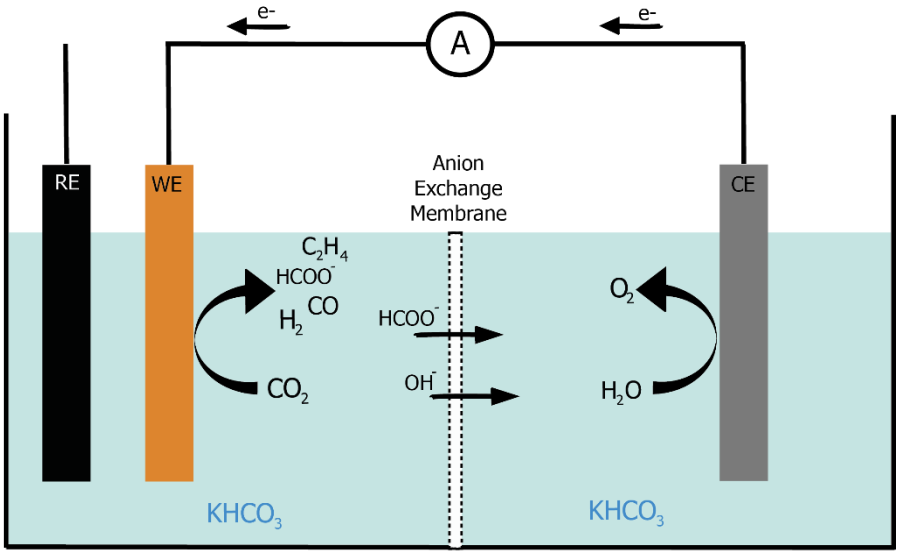

Figure 4. *Schematic representation of an H-cell. The electrochemical cell used for the CO_2 Reduction Reaction in this research.*

CO_2 is bubbled through the catholyte, enabling it to dissolve and get in contact with the working electrode, where the reduction towards the reaction products takes place. However, since CO2 has a low solubility in water, mass transport limitations are observed in the H-cell.[20] This limits the current density that can be achieved. In the CO_2RR, gaseous products, such as carbon monoxide, methane and ethylene, and liquid products, such as formate and ethanol, can be produced. Oxidation occurs at the counter electrode, forming oxygen from water.

2.2. Selectivity problem

Thus far, at least 17 different products have been reported in the CO_2 Reduction Reaction, all with similar equilibrium potentials. In table 1, relevant half reactions are summarized, together with their equilibrium potentials and the major product. The reactions can be classified by the amount of electrons used in the catalysis, e.g. six-electron reactions towards methane or methanol or the eight-

electron reaction towards ethylene. Unfortunately, unwanted hydrogen gas is also formed with two electrons, making it a competitive reaction: the Hydrogen Evolution Reaction (HER).

Table 1. *The equilibrium potentials for the reduction reactions occurring during the CO_2RR. Duplicated from Nitopi et al.*[21]

Reaction	E^0/[V vs RHE]	(Product) Name, abbreviation
$2H_2O \rightarrow O_2 + 4H^+ + 4e^-$	1.23	Oxygen Evolution Reaction, OER
$2H^+ + 2e^- \rightarrow H_2$	0	Hydrogen Evolution Reaction, HER
$xCO_2 + nH^+ + ne^- \rightarrow product + yH_2O$		*CO_2 Reduction, CO_2R*
$CO_2 + 2H^+ + 2e^- \rightarrow HCOOH_{(aq)}$	−0.12	Formic acid
$CO_2 + 2H^+ + 2e^- \rightarrow CO_{(g)} + H_2O$	−0.10	Carbon monoxide
$CO_2 + 6H^+ + 6e^- \rightarrow CH_3OH_{(aq)} + H_2O$	0.03	Methanol, MeOH
$CO_2 + 4H^+ + 4e^- \rightarrow C_{(s)} + 2H_2O$	0.21	Graphite
$CO_2 + 8H^+ + 8e^- \rightarrow CH_{4(g)} + 2H_2O$	0.17	Methane
$2CO_2 + 2H^+ + 2e^- \rightarrow (COOH)_{2(s)}$	−0.47	Oxalic acid
$2CO_2 + 8H^+ + 8e^- \rightarrow CH_3COOH_{(aq)} + 2H_2O$	0.11	Acetic acid
$2CO_2 + 10H^+ + 10e^- \rightarrow CH_3CHO_{(aq)} + 3H_2O$	0.06	Acetaldehyde
$2CO_2 + 12H^+ + 12e^- \rightarrow C_2H_5OH_{(aq)} + 3H_2O$	0.09	Ethanol, EtOH
$2CO_2 + 12H^+ + 12e^- \rightarrow C_2H_{4(g)} + 4H_2O$	0.08	Ethylene
$2CO_2 + 14H^+ + 14e^- \rightarrow C_2H_{6(g)} + 4H_2O$	0.14	Ethane
$3CO_2 + 16H^+ + 16e^- \rightarrow C_2H_5CHO_{(aq)} + 5H_2O$	0.09	Propionaldehyde
$3CO_2 + 18H^+ + 18e^- \rightarrow C_3H_7OH_{(aq)} + 5H_2O$	0.10	Propanol, PrOH
$xCO + nH^+ + ne^- \rightarrow product + yH_2O$		*CO Reduction, COR*
$CO + 6H^+ + 6e^- \rightarrow CH_{4(g)} + H_2O$	0.26	Methane
$2CO + 8H^+ + 8e^- \rightarrow CH_3CH_2OH_{(aq)} + H_2O$	0.19	Ethanol, EtOH
$2CO + 8H^+ + 8e^- \rightarrow C_2H_{4(g)} + 2H_2O$	0.17	Ethylene

The selectivity is dependent on the binding energies of CO_2RR intermediates and adsorbed hydrogen on different catalyst metals, as shown in Figure 5. Metals with a positive binding energy for CO_2 (e.g. Cd and Sn) bind CO_2 weakly and therefore produce formate. Metals with a positive binding energy for CO (Ag, Au and Zn) are capable of binding CO_2 and reducing it to CO, but they release CO too easily to reduce it further. Therefore, these metals produce primarily CO. The third group of metals is the metals with a negative binding energy for hydrogen (Ni, Pd and Fe). These metals strongly release H_2 in the Hydrogen Evolution Reaction.[22]

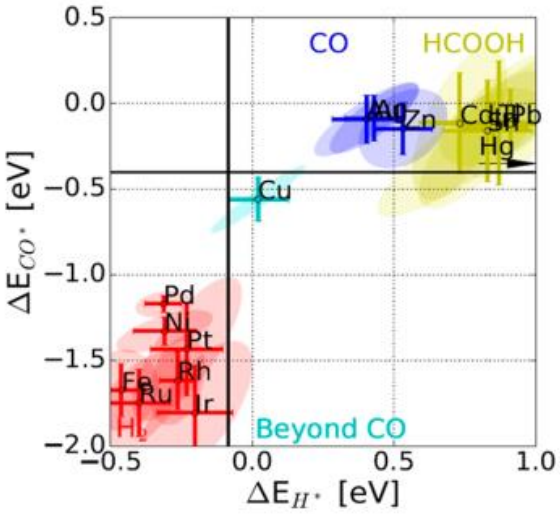

Figure 5. *CO_2 reduction metal classification. Duplicated from Bagger et al.*[23]

Copper is the only metal that can produce significant amounts of valuable products that require C-C coupling, such as hydrocarbons and alcohols. This ability to form C-bonds is due to copper's negative adsorption energy for *CO but positive adsorption energy for *H (see Figure 5).[21] Hydrocarbons and alcohols, also called C_{2+} products, are of special interest due to their high energy density and high economic value.[24] However, copper is unselective, and in addition to C_{2+} compounds, less valuable products such as CO, hydrogen and methane are formed.[10] Therefore, several efforts have been made to increase the selectivity of copper-based electrocatalysts, including the use of bimetallic systems,[25,26] oxide-derived copper,[12,13,27] and tuning the morphology of the catalyst[14,15]. These three improvement strategies will each be discussed in the following subsections.

2.2.1. Bimetallic copper systems

Bimetallic systems are frequently used as a method to increase the selectivity of a copper catalyst by generating an in situ source of CO. CO is the main intermediate in the CO_2RR towards C_{2+} products, but has a poor solubility in aqueous solutions.[28] Therefore a low current density is observed, however, if a co-catalyst produces CO selectively, the mass transport limitations could be decreased. As a result, this in situ produced CO can then be reduced to hydrocarbons or alcohols on copper nanoparticles.[29] This tandem catalysis is also known as the spillover effect.

Addition of various metals to Cu-based electrocatalysts have been investigated for synergistic effects. Upon intimate mixing of two metals, the electronic structures can be changed, thus creating new active sites.[2] Especially the addition of gold and silver are state-of-the-art for the production of CO.[30–32] For example, Ting *et al*. synthesized a Cu-Ag catalyst and observed a fivefold improvement in ethanol production. They propose that the excess of CO formed by silver is aiding this transition from CO_2 towards ethanol.[17] Cu-Au alloys developed by Jia *et al.* were selective towards alcohols in aqueous systems.[33] And Huang *et al*. report a 3.4-fold enhancement in faradaic efficiency toward C_2H_4 and a doubled activity when comparing Ag/Cu nanocrystals to the monometallic system.[25]

Beside Ag and Au, also Zn is known to selectively produce CO.[26] Furthermore, it is low-cost, non-toxic and the 23th most abundant element on Earth.[34] Furthermore, the atomic radii of zinc and copper are similar (139 and 140 pm, respectively), making them great candidates for alloys with multiple mixed states.[35] Therefore, the chemical composition and degree of alloying can be varied to a great extent. This provides ample opportunity for tuning the electronic properties of both metals, which might benefit their electrocatalytic CO_2RR performance.

However, challenges can be expected when using zinc in the CO_2RR. One of the biggest challenges is the dissolution of zinc, which can be explained with the Pourbaix diagram, see figure 6. The standard reduction potential of zinc is -0.76 V vs. SHE, causing zinc to be unstable in H_2O and dissolve at open circuit. This results in restructuring of zinc particles during catalysis in aqueous solutions. The dissolution of the zinc catalyst decreases the stability of the catalyst, but seems to have no influence on the product formation in the CO_2RR.[36] Another disadvantage is the high overpotentials required for zinc to be active in the CO_2RR.[26] Therefore, competition with the hydrogen evolution reaction is observed.

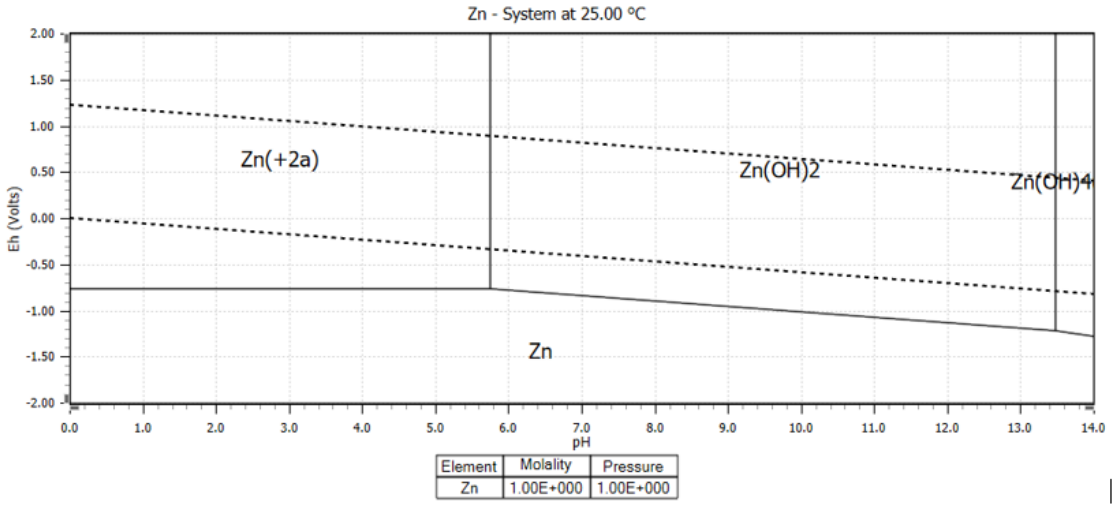

Figure 6. *Pourbaix diagram of Zn at standard conditions.*

Cu/Zn bimetallic systems

The combination of copper and zinc for the reduction of CO_2 has gained the interest of many researchers recent years, both in simulations and in experimental work. The synergistic sites of CuZn nanoparticles are considered to have a great influence on the adsorption of CO and therefore play a big role in the selectivity of the CO_2RR.[37] CuZn bimetallic catalysts with faradaic efficiencies outshining monometallic copper systems have been reported.[22] Furthermore, CuO and ZnO are often used together, where CuO is used as a promoter in the methanol production of ZnO.[38] Not only C_1 products have been reported in literature, also increased faradaic efficiencies towards C_{2+} products have been ascribed to the combination of copper with zinc. Recently, Dongare *et al.* combined CuO and ZnO via co-precipitation. They saw the faradaic efficiency toward ethanol increase from 9 % to circa 22.3 % when 10 w% ZnO is added. This effect is ascribed to the abundance of CO in solution produced by zinc, and the ability of copper to bind CO and CH, forming *COCH.[13]

Alloys

When varying the ratio of zinc and copper, different alloy phases can be formed, because the parent structures of the two metals differ (hexagonal close-packed for Zn versus cubic close-packed for Cu). The different possible alloy phases are depicted in Figure 7 and called intermetallic compounds.[39] The changes entailing intermetallic compounds in electronic structure, chemical bifunctionality and geometric strain allow for modified chemical binding of intermediates on the catalyst surface.[40]

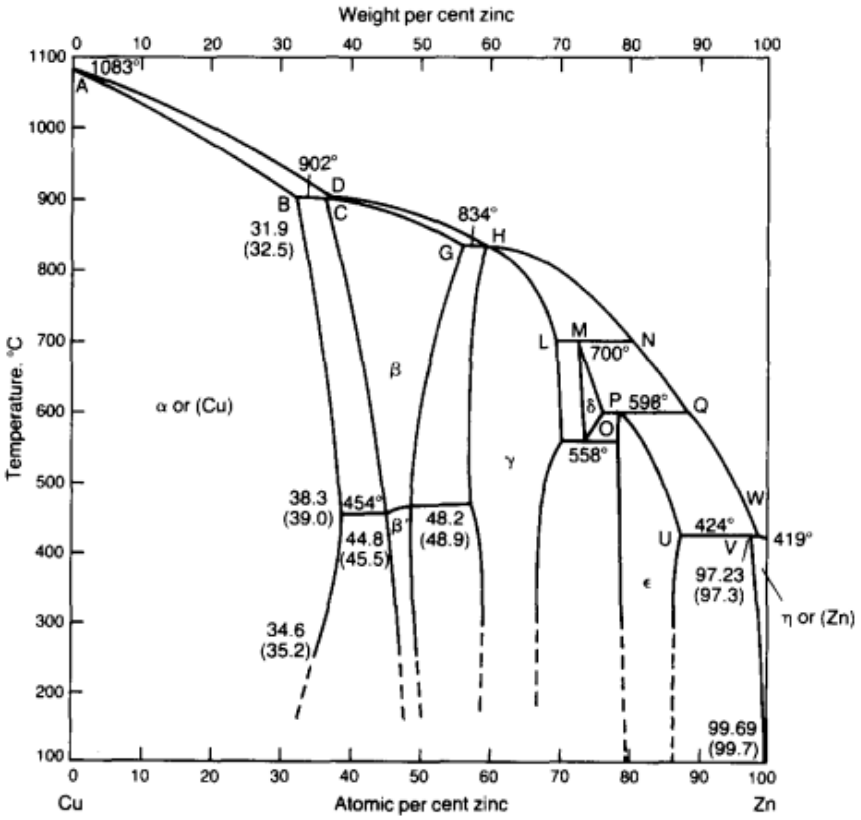

***Figure 7**. The equilibrium phase diagram for Cu/Zn, showing five different stable CuZn alloy phases called α, β, γ, δ, ε, η. Duplicated from M. Ahlers.*[41]

2.2.2. Oxide-derived electrodes

Oxide-derived electrodes are widely studied for their improved CO_2RR performance as compared to the pure metals. However, a detailed mechanism of oxide-derived species and their performance in the CO_2RR is still under debate. One of the often mentioned explanations for the improved performance is the increased surface area of oxide-derived particles, containing more defects, which increases their activity. In turn, more protons are consumed, which increases the local pH. This suppresses the hydrogen evolution reaction and thus enhances the selectivity for C_{2+} products.[12]

Oxide-derived copper shows an improved catalytic performance as compared to its metallic counterpart.[12] In research conducted by Ren *et al*., the faradaic efficiency of ethylene and ethanol were increased from 13.8% and 0% to 39% and 16%, respectively, when going from metallic copper to oxide-derived copper electrodes.[19] The study was executed with Cu_2O films of different thicknesses and analysed by SEM, XRD and in-situ Raman spectroscopy. They suggest a Cu^0 oxidation state to be responsible for their results, since the surface of their Cu_2O electrode is reduced and remains metallic under CO_2RR conditions. However, research performed by de Luna *et al*. on oxide-derived copper catalysts supported by DFT calculations suggests that Cu^+ is an important species in ethylene formation, due to its stabilization of the OCCOH* intermediate.[42]

Not only oxide-derived copper, but also oxide-derived zinc shows this improved catalytic performance. A more detailed explanation of this phenomenon in oxide-derived zinc electrodes is described in the review written by Solomon *et al*.[11] Herein, it is explained that the hydrogenation of CO on a ZnO-derived catalyst favours methanol production, in which the C-O bond is retained, instead of the expected methane, in which the C-O bond is broken. The reason for this unusual retaining of the C-O

bond is that CO binds to the coordinatively unsaturated zinc ion as a sigma donor. This eventually causes the C-O bond to be stronger and results in methanol formation.

2.2.3. Morphology

A third parameter that is important for tuning the electrocatalytic performance is the electrode morphology. It is known that by nanostructuring, a higher roughness and surface area of the catalyst particles are introduced. Furthermore, more defect sites are generated, which have been shown to possess a higher binding energy for CO_2 and an enhanced catalytic conversion towards C_{2+} products.[14] Recently, da Silva *et al.* researched the effects of chemical composition and surface morphology on the CO_2RR of CuZn electrodes. They found that nanostructure shape had a bigger influence on the production of C_{2+} products than chemical composition.[15] The nanocubes, exposing the (100) facet of copper, enhanced the C_{2+} production most, which is in agreement with other literature reports on Cu particles.[9,43]

Since nanostructured zinc electrocatalysts are already investigated in our group, we can expand on earlier obtained knowledge. Han *et al*. synthesized ZnO nanorods of different size and thickness, and found that reduction changed the morphology immensely.[44] The thinnest nanorods became sponge-like after reduction in CO_2 saturated 0.5 M $KHCO_3$, while the middle and thickest nanorods maintained their structure. However, when reduced in CO_2 saturated 0.1 M $KClO_4$, nanoplates were formed. Of all morphologies tested in this research, these nanoplates showed the highest faradaic efficiency for CO.

Unfortunately, performing morphological studies can often prove difficult. First of all, imperfections in the structure of catalyst particles make it difficult to disentangle shape effects from other effects like the amount of surface atoms and other defect sites.[21] Secondly, the catalyst structure is often not stable during catalysis.[44] Whereas the morphology can be analysed before and after catalysis, studying it *in situ* technique is extremely challenging.[45,46]

3. Methods

This chapter describes the chemicals and methods that were used during this research. First, the chemicals with purification and vendor will be specified. Subsequently, the synthesis methods, galvanic replacement and drop casting, that are performed are described. Lastly, the characterization methods and details of electrochemical measurements will be discussed.

3.1 Chemicals

Copper(II) nitrate hydrate (99 %), copper(II)chloride dihydrate (99.0 %), zinc nitrate hexahydrate (>99%), sodium hydroxide (97.0 %), NH_2OH*HCl (99.995 %), 2-propanol (99.5 %), potassium bicarbonate (99.9 %), Chelex® 100 sodium form, 50 – 100 mesh (dry) and Nafion® 117 solution (5 % in a mixture of lower aliphatic alcohols and water) were purchased from Sigma Aldrich. Sodium dodecyl sulphate (99%) was obtained from Acros Organic and ethanol (99.5%) and acetone from VWR chemic. Kalium chloride (>=99%) was purchased from Fisher Chemical and hexamethylenetetramine (99%) and sodium nitrate (99.0 %) from Thermoscientific,

All chemicals were used without further purification.

3.2. Galvanic Replacement

Zinc foil (from Goodfellow, 0.025 mm in thickness) was cut into discs of approximately 4 cm^2. They were cleaned by rinsing them three times alternating ethanol and MilliQ water (taken from Direct G^R 3UV machine), followed by drying under ambient conditions. To submerse the zinc foil evenly in solutions, a customized holder was made, see figure 8. Herein, the foil is held in place by pressing it against a glassy carbon disc and sealed leak-tight using an O-ring.

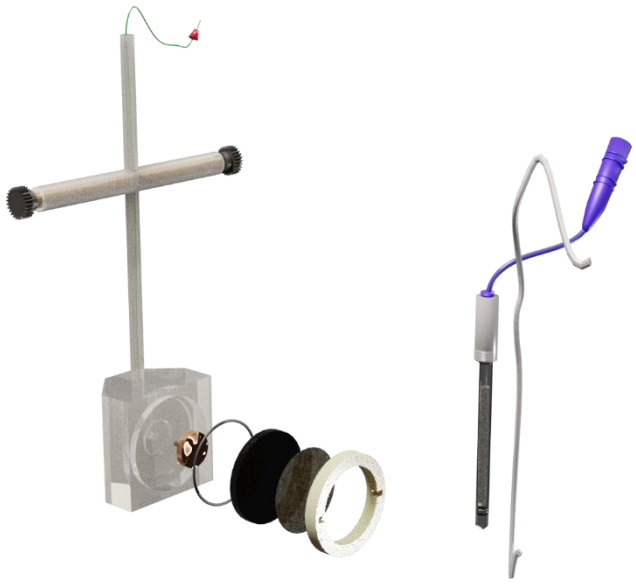

Figure 8. *Representation of the holder used to submerse the zinc foils in solution.*

The holder was put in a beaker containing 100 mL of 100 mM $Na(NO_3)$. To fully reduce the zinc and measure the resistance, an linear sweep voltammetry (LSV) from 0 to -0.577 V, electrochemical impedance spectroscopy (PEIS), then cyclic voltammetry (CV) from -0.577 V to -1.377 V and

chronoamperometry (CA) on -1.377 V, all versus RHE, were executed. Hereafter, the reduced zinc foil was immersed into a $Cu(NO_3)_2$ solution for two minutes to exchange Zn for Cu. To vary the amount of copper exchanged, the $Cu(NO_3)_2$ concentrations were systematically varied from 0 – 10 mM. The colour of the foil after this submersion varied from yellow/brown to black depending on the molar concentration of the $Cu(NO_3)_2$ solution, see appendix A.

3.3. Oxide-derived Cu2O-ZnO-based electrodes

ZnO nanorod synthesis

ZnO nanorods were synthesized via a hydrothermal synthesis method as described by Han *et al*.[44] 0.74 g $Zn(NO_3)_2*6H_2O$ and 0.35 g hexamethylenetetramine were dissolved in 50 mL deionized water, yielding a 0.05 M and 0.05 M solution. Teflon liners were filled with 10 mL solution and sealed and heated in an autoclave at 85°C for four hours. Afterwards, the white precipitate was collected and washed three times with MilliQ and once with ethanol. Thereafter, they were left to dry under ambient conditions.

Cu_2O nanocubes synthesis

Cu_2O nanocubes were synthesized using the method described by Huang *et al*.[47] 89.2 mL deionized water was added to a 250 mL round bottom flask and heated to 33°C in a water bath. 5 mL of 0.1 M $CuCl_2$ solution and 0.87 g sodium dodecyl sulphate surfactant were added and dissolved under stirring at 450 RPM. After this dissolution, 1.8 mL of 1 M NaOH was added and the solution rapidly turned blue due to formation of $Cu(OH)_2$ seeds. Stirring was increased to 1000 RPM and after two minutes, 4 mL of 0.1 M $NH_2OH*HCl$ solution was introduced. After two minutes, the stirring was stopped. The colour changed from blue to green to yellow to orange in circa six minutes. After growing the nanocrystals for one hour, the mixture was centrifuged at 4500 RPM for five minutes. The supernatant was decanted and the precipitate was washed three times with 50 mL of a 50:50 mixture of MilliQ water and ethanol. Lastly, the Cu_2O cubes were washed once with pure ethanol and dried under ambient conditions.

Working electrode preparation

Glassy carbons (SIGRADUR K-discs from HTW HochtemperaturWerkstoffe GmbH, diameter 30 mm, thickness 2mm) were cleaned by rinsing with sequentially deionized water, ethanol and acetone. Then, they were polished with sequentially 1, 0.25 and 0.05 µm Polish MetaDiTM and sonicated for 15 minutes.

To prepare the catalyst ink, 4 mg nanoparticles (either Cu_2O nanocubes or ZnO nanorods) were added to a vial. 1.6 mL MilliQ water, 300 µL 2-propanol and 100 µL 5 wt% Nafion solution were added. The resulting ink, with a catalyst loading of 0.5 mg in 2000 µL ink, was sonicated for 15 minutes and dropped on a glassy carbon substrate and dried under ambient conditions. A total of 250 µL of this ink in different Cu_2O:ZnO ratios was drop casted onto each glassy carbon. In appendix E, a list of all sample names with different Cu_2O:ZnO ratios is given.

Washing treatment

After catalysis all drop casted electrodes are disposed of salts by rinsing them with MilliQ and leaving them in MilliQ water. Thereafter, the MilliQ is decanted and they are left to dry under ambient conditions.

3.4 Characterization

Scanning Electron Microscopy

Scanning electron microscopy (SEM) and energy dispersive X-Ray Spectroscopy (EDX) of the galvanic replaced electrodes were performed on a Phenom Pro Thermo Fisher.

SEM-EDX micrographs and elemental maps of the oxide-derived particles were made on a Zeiss EVO 15 instrument equipped with a secondary electron detector, operating at 400 pA and 10.0 kV for imaging and 20.0 kV for elemental maps

SEM micrographs were taken on a Zeiss Gemini 450 equipped with Inlens detector and operated at 10 kV and 500 pA

X-Ray Diffraction

X-Ray Diffraction (XRD) measurements were carried out on a Bruker D2 Phaser with a Co Kα X-ray wavelength of 1.79026 Å.

Ion Coupled Plasma

Ion coupled plasma was performed on a PerkinElmer Optima 8300 ICP-OES with a PerkinElmer S10 autosampler, the software used was Syngistix.

3.5 Electrochemical measurements

Catalytic testing was performed in a custom-made H-cell. The cathodic side and the anodic side were separated by an anion exchange membrane (Selemion membrane from ACG engineering) . At the anodic side, a counter electrode consisting of glassy carbon and carbon paper (TGP-H-060 from Toray) were used. At the cathodic side, the Ag/AgCl reference electrode (saturated in 3 M KCl, Metrohm) and the working electrode are present. Both the anolyte and the catholyte consist of 15 mL of 0.1 M $KHCO_3$ solution. The electrolyte was purged for 30 minutes before each measurement with 20 mL/min Ar and CO_2 gas for the anolyte and catholyte, respectively.

Electrochemical Impedance Spectrometry (EIS) was performed before each measurement to determine the cell resistance, typically around 30 Ω. All potentials were converted from versus the Ag/AgCl reference electrode to RHE and iR corrected according to equation 1.

$$E_{IR}\ (vs.RHE) = E_{Ag/AgCl} + 0.209 + 0.059 * pH - iR \quad (1)$$

Where $E_{Ag/AgCl}$ is the measured potential, I is the current and R is the measured resistance. The pH of the CO_2-saturated 0.1 M $KHCO_3$ electrolyte used is 6.8.

The gaseous products were analysed using an on-line gas chromatograph (Compact GC4.0 Global Analyzer Solution GAS) with three detectors (a Thermal Conductivity Detector, a Flame Ionization Detector and a Flame Ionization Detector with a methanizer). Liquid products were measured by hydrogen nuclear magnetic resonance spectroscopy (H1-NMR on the Varian MRF 400 MHz spectrometer). The faradaic efficiencies were calculated with use of equation 2, where the moles of products for gaseous products were calculated with equation 2.1 .

$$FE(\%) = \frac{n_x * F * [moles\ of\ products]}{Q} * 100\% \quad (2)$$

In which n_x is the amount of electrons needed to form product x, F is the faradaic constant (96 485 C/mol) and Q is the charge (C) consumed.

$$[moles\ of\ product] = \frac{C_x * q}{V_m} \quad (2.1)$$

Where C_x is the response factor in ppm, q is the gas flow rate (20 mL/min) and V_m is the total volume of an ideal gas (22.4 m^3).

The liquid products were calculated by making use of an internal standard and acknowledging earlier measurements.

4. Results

This chapter will describe the results of both the conducted research on galvanic replaced electrodes and oxide-derived particles. In section 4.1, the galvanic replaced electrodes are discussed. This section will be divided in six parts: the catalyst characterization, the activity, the selectivity and the stability results, a discussion on the roughness effect and a short conclusion and discussion on the method. In section 4.2, the results of the oxide-derived electrodes is reported. This method has a few advantages over galvanic replacement, namely the controllable morphology and multiple oxidation states.

4.1. Galvanic replacement

Galvanic replacement is an electroless plating technique in which atoms of a less noble metal are displaced by a more noble metal.[48] In our case, copper will take the place of zinc in a zinc nanostructure. This technique combines a simple synthesis with a composition that puts copper and zinc atomically close to each other.[49]

4.1.1. Catalyst characterization

Multiple electrodes are synthesised using the galvanic replacement technique: GR_0.5, GR_2.9, GR_6.2, GR_6.7 and GR_12.5, where the number indicates the atomic percentage of copper as determined by SEM-EDX (see section 4.1.2. Morphology effects).

SEM-EDX

The morphology of the zinc foils changed drastically upon immersion in the copper solution, see figure 9. We observed two main structural changes. First, the foil was etched, resulting in formation of cracks. Second, round, pebble-like structures had grown on top of the foil and in between the cracks. EDX results verify these pebble-like structures to be copper, see appendix B. The copper content was determined by SEM-EDX to be 0.5, 2.9, 6.7, 6.2 and 12.5 atomic% copper when 1 mM, 2.5 mM, 5 mM, 7.5 mM and 10 mM copper solution were used in the synthesis, respectively, see table 2. Since the EDX has a penetration depth of circa 2 µm, this weight percentage only relates to the upper 10% on the surface of the electrode.

Table 2. *The volumes of copper solution used to prepare multiple molar concentrations of copper solution.*

Sample name	mM copper solution made	mL of 100 mM $Cu(NO_3)_2*3H_2O$ used	mL of deionized water used
GR_0.5	1	1	99
GR_2.9	2.5	2.5	97.5
GR_6.7	5	5	95
GR_6.2	7.5	7.5	92.5
GR_12.5	10	10	90
GR03	100	100	0

A correlation is seen between the size of the pebbles and the amount of copper in the sample as determined with EDX. An increased amount of copper resulted in a larger pebble size. As can be seen in the zoomed-in figures, the structure of the pebbles becomes cauliflower-like when reaching a size larger than 100 nm. Cauliflower structures are a well-known shape for copper particles and have been mentioned before in electroless deposited structures.[50] In the electrode with least and most copper content, the pebbles are evenly distributed and roughly monodisperse. In the samples in between, though, we observe both small pebbles as in GR_0.5 and large pebbles as in GR_12.5. The smaller

particles are mostly concentrated in the cracks and deeper in the foil, whilst the top layer consist mostly of larger particles, as can be seen in figure 9 GR_6.7.

When even higher copper concentrations than 12.5 atomic% were used, dendrites consisting of copper and big chunks consisting of zinc, both of circa 50 µm, were recognized, see appendix B. These larger particles cause the zinc and copper to be farther away from each other and are therefore less interesting when looking at synergistic effects. Catalytic testing of the sample confirmed this hypothesis by showing significant hydrogen formation.

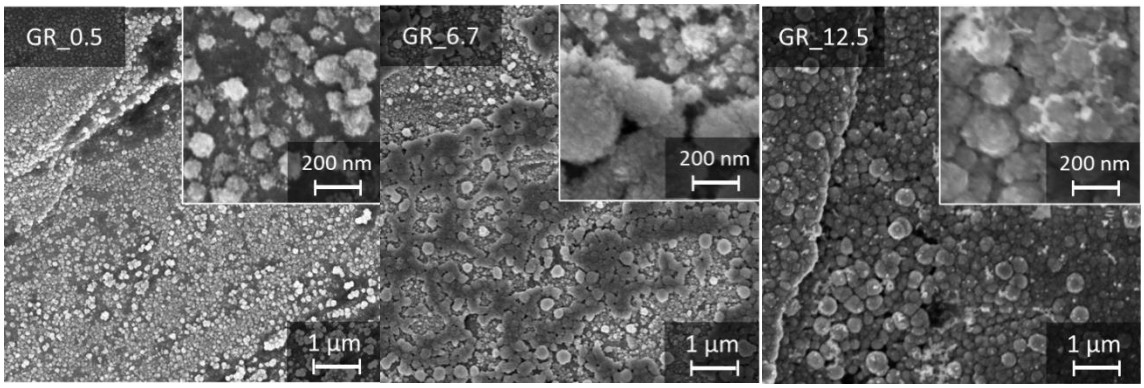

Figure 9. *SEM images from GR_0.5, GR_6.7 and GR_12.5 before catalysis.*

XRD

The synthesized electrodes were observed with XRD before catalysis to determine the catalyst oxidation state and discover if the electrodes consist of zinc foil with copper on top or if an intermetallic copper/zinc alloy phase was present. As can be seen in figure 10, the diffractograms correspond to that of the zinc foil and thus to metallic zinc. At a 2θ of 58° a little peak is observed and at circa 75°, two little bumps are seen. These correspond to monometallic copper,[51] and not to an intermetallic phase of zinc and copper as described in the theory section 2.2.1. The peaks indicating monometallic zinc shift slightly per sample, however, since the foils were not all perfectly flat while measuring the XRD, we believe this to be the result of differences in measuring height in the XRD and not of an alloy formation. From this diffractogram we can conclude that metallic copper structures have grown on top of the zinc foil, but copper has not infiltrated the hexagonal structure of zinc.

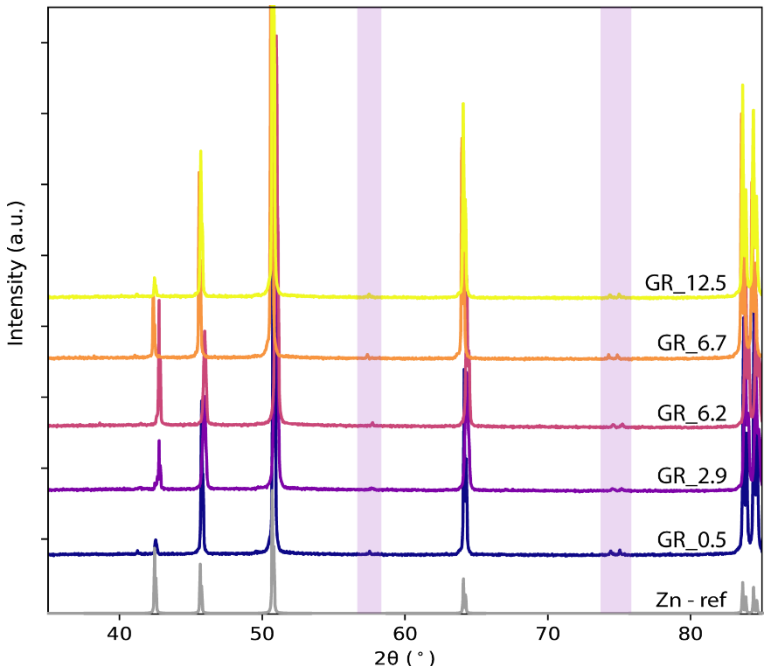

Figure 10. *The normalized diffractograms of the synthesized electrodes before catalysis with increasing copper content from bottom to top.*

4.1.2. Activity

The electrodes with different Cu:Zn ratios were catalytically tested to obtain results on activity, selectivity and stability during a measurement. The measurements were conducted for two hours on -1.39 V, the potential with the most CO formation by zinc foil. This potential is determined without correcting for the resistance in the cell.

To compare the activity of the synthesised electrodes, the total current densities of all samples were analysed, see figure 11. The current is stable for every sample after approximately 30 minutes. Interestingly, the synthesised electrodes with both zinc and copper on the surface all show higher current densities than both monometallic counterparts. This suggests that combining copper with zinc increases the activity of the catalyst. The synthesised electrodes themselves are ordered in such a way that with increasing copper content, increasing activity is observed. This could indicate that a synergistic effect between the copper and zinc occurs.

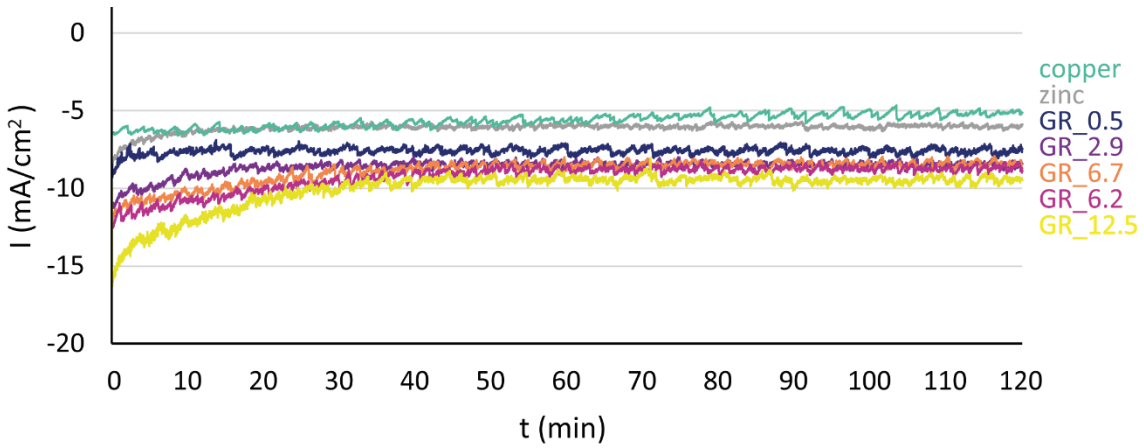

Figure 11. *The total geometric current density of all synthesised electrodes and the two reference electrodes (zinc and copper foil) versus time.*

4.1.3. Selectivity

Figure 12 shows the faradaic efficiency for different products obtained during catalysis. All synthesised electrodes exclusively produce hydrogen and carbon monoxide, except for the copper foil. Interestingly, no C_{2+} products are produced when copper is added to the zinc foil. It is possible that we did not reach potentials high enough to form C_{2+} products, since no correction for the resistance in the cell was used. We expect the iR-corrected potentials to be around -0.9 to -1.0 V, assuming a resistance of 30 Ohms. C_{2+} products are known to be formed in significant amounts at potentials of circa -1.1 V. However, the copper foil itself does produce C_{2+} products at this same potential. Another explanation for the lack of C_{2+} products is the formation of an alloy phase giving rise to a change in the product distribution. Since the product distribution in the CO_2RR of all Zn/Cu alloy phases is unresolved, more knowledge is needed in order to draw a clear conclusion.

The increase of selectivity towards CO when bimetallic systems with copper are used has been observed before. Zhiyuan *et al*. propose that the oxygen affinity of copper helps stabilizing the *COOH intermediate.[16] Since they use small amounts of copper, CO gets released before further protonation can occur.

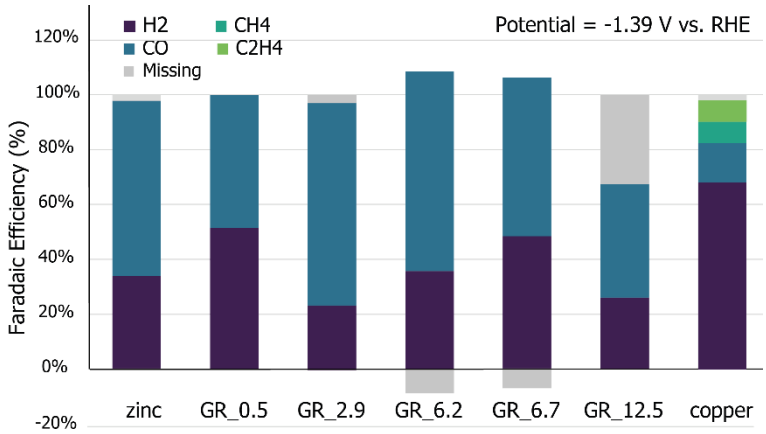

Figure 12. *Faradaic efficiency per sample, measured at -1.39 V vs RHE, not iR-corrected.*

No clear trend is observed in terms of CO : H_2 ratio. However, when the partial current density for CO is plotted against the copper content of the electrodes, an optimum atomic composition for the surface is observed, see Figure 13. 2.9 and 6.2 atomic percentage of copper (in the upper 10% of the electrode) show the highest partial current density for CO formation with over 6 mA/cm^2. A hypothetical Lorentz fit, as calculated by Origin is drawn in the graph to show the possible maximum. The calculated values are depicted in appendix C.

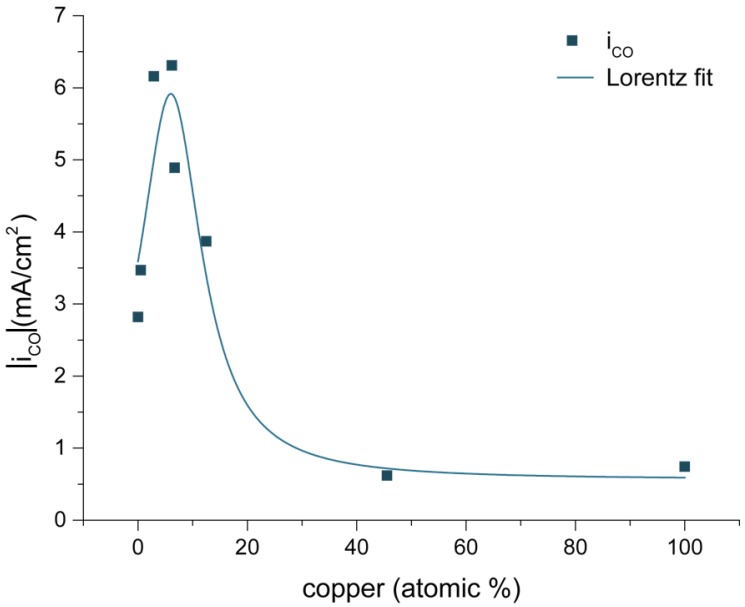

Figure 13. *The partial current density for carbon monoxide in mA/cm^2 plotted against the weight percentage of copper present in each electrode as determined with EDX.*

The maximum can be the result of the Cu:Zn ratio, but other explanations need to be taken into account as well. Firstly, the morphology of the foil might be altered during the synthesis or during catalysis, possibly giving rise to an increased roughness of the surface. Moreover, mobility of copper and zinc species under CO_2RR conditions might induce redistribution of both elements and possibly cause alloy formation, giving rise to intermetallic phases that possess different reactivity. To obtain more information on these effects, characterization after catalytic testing was performed.

4.1.4. Stability

XRD

When we look at the diffractogram after catalysis (Figure 14), the same peaks are observed as in the diffractogram before catalysis. Interestingly, additional peaks have appeared at 44° and 49°. These correspond to the epsilon phase in a Cu/Zn alloy, with around 80% Zn and 20% Cu.[52] Thus, it appears that the epsilon alloy phase has formed in certain parts of the electrode. As clear in the zoomed-in diffractogram in Figure 14, the peaks corresponding to the epsilon phase intensify with increasing copper content. Hence, we can conclude that copper is integrated in the hexagonal crystal lattice of zinc, resulting in a crystal structure combination of the zinc and the copper/zinc epsilon phase.

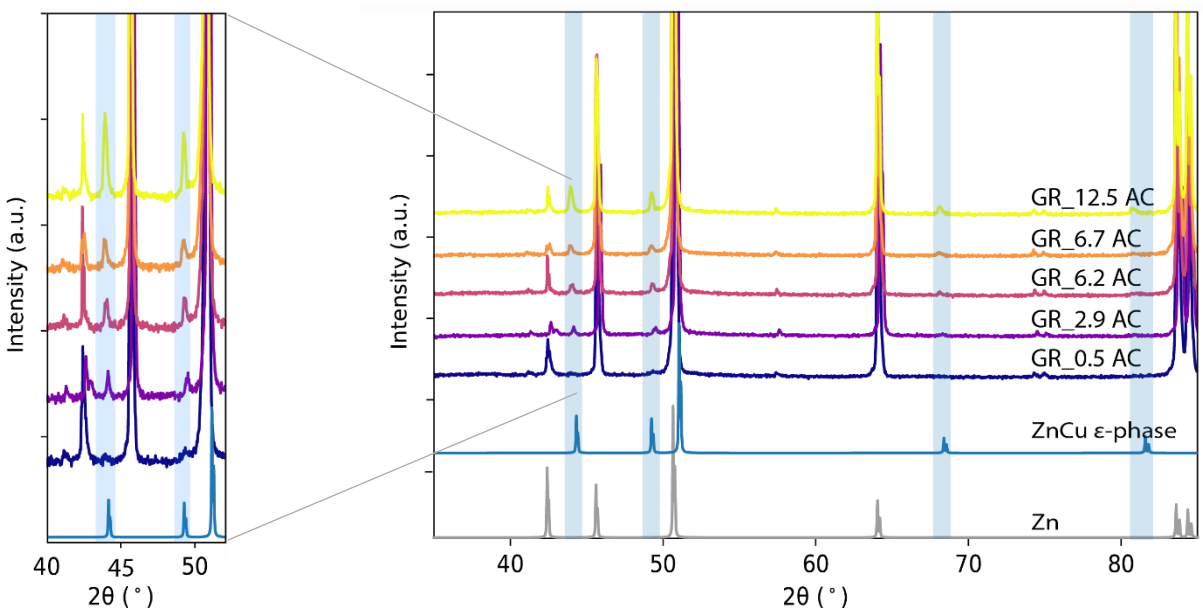

Figure 14. *The normalized diffractograms of the synthesized electrodes after catalysis with increasing copper content from low to high. The blue strokes indicate the 2ϑ at which the epsilon phase of Cu:Zn alloys is observed.*

SEM-EDX

After catalysis, platelets are observed in the electrodes, see Figure 15. Plate-like structures have been reported in literature when the ε-phase of Zn-Cu alloys is observed.[53–55] However, we observe them in GR_0.5, which has the least amount of copper, and in GR_12.5, with the most amount of copper, but not in GR_6.7, with an intermediate amount of copper. Thus, the formation of platelets has no correlation with the Cu:Zn ratio. If the platelets were to be the ε-phase of Zn-Cu alloys, we would expect the amount of platelets to increase with increasing copper content as we saw in XRD measurements that the ε-phase of Zn-Cu alloys show a positive correlation with the copper content. Furthermore, EDX measurements confirm the platelets to consist of zinc and oxygen and the small pebbles seen in between the platelets to be copper mixed with zinc.

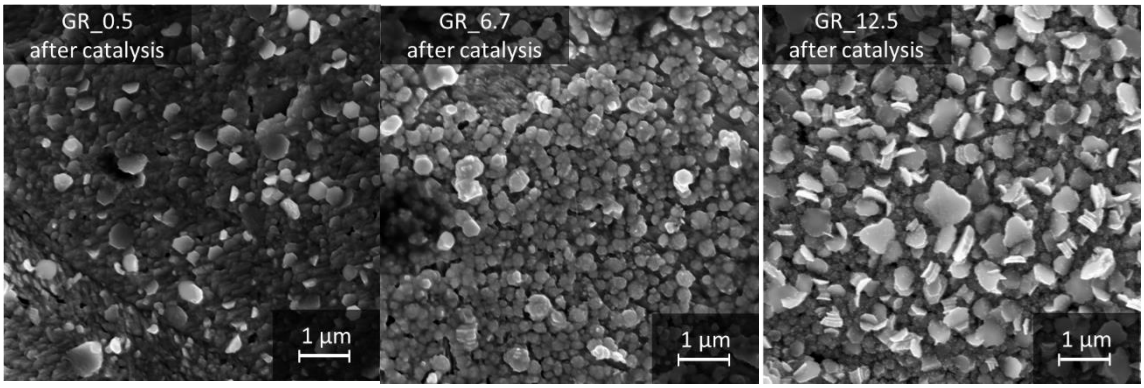

Figure 15. *SEM images from GR_0.5, GR_6.7 and GR_12.5 before and after catalysis.*

The change in morphology during catalysis is often observed and is most likely the result of dissolution-redeposition mechanism.[37] This is confirmed by ICP data, where zinc is observed in the electrolyte, indicating the dissolution of zinc during catalysis.

4.1.5. Effect of surface roughness

An increase in surface roughness can result in a higher selectivity towards C_{2+} products.[56–58] Therefore, we would expect more C_{2+} products for cauliflower shapes than for nanospheres, since cauliflowers have a higher roughness factor, i.e. more catalytically active sites per geometric unit of area than nanospheres. This means that it is unsure if the optimum in CO production found is due to the Cu:Zn ratio or due to the roughness effect. To investigate the roughness of our different samples, the electrochemical surface area (ECSA) of the samples needs to be determined.

The only method for ECSA determination applicable to our samples is double layer capacitance, which is a common method for copper samples. However, when trying to find a non-faradaic region for the zinc foil, it was discovered that there is no such region for zinc. The performed measurements can be found in the appendix D.

4.1.6. Discussion of galvanic replacement

The copper was introduced in the zinc lattice structure, giving rise to the intermetallic Cu:Zn compound. An optimum partial current density of CO was observed when 2.9 - 6.2 atomic% of copper is plated electroless on zinc foil. This optimum is most likely caused by a promoting and a deteriorating effect counteracting. The promoting effect could be an increase in electrochemical surface area, resulting in additional CO production. However, since the electrochemical surface area is undetermined in this project, further research is necessary.

A suggestion for the deteriorating effect is the addition of copper, increasing hydrogen formation. XRD confirmed the development of the Zn/Cu epsilon phase to grow with increasing copper concentration. Because copper is known for significant hydrogen formation, we expect the presence of the Zn/Cu epsilon phase to cause a higher hydrogen formation. To get more knowledge on the product distribution of the Zn/Cu epsilon phase in the CO2RR, a homogeneous Zn/Cu epsilon phase electrode should be synthesised and catalytically tested.

4.2. Oxide-derived Cu_2O-ZnO-based electrodes

In galvanic replacement, we have no control over the catalyst morphology and (metallic) oxidation state. In the previous section, it was described that only hydrogen and carbon monoxide were produced in the CO_2RR using the galvanic replaced electrodes. C_{2+} products were absent, even when copper, which is known for being the only metal to produce a significant amount of C_{2+} products in the CO_2RR, was introduced in the crystal lattice of zinc. As described in the theory in sections 2.2.2. and 2.2.3., apart from using bimetallic versus monometallic particles, the selectivity of electrodes in de CO_2RR can be tuned by changing the morphology or using oxide-derived particles instead of metallic particles.

The drop casting method allows for an electrode with a quantified amount of dispersed nanoparticles.[59] Since these nanoparticles are synthesized beforehand, it gives complete control over the morphology. Specifically, Cu_2O nanocubes and ZnO nanorods were used which we reduce beforehand, giving us oxide-derived species. The cubic shape of copper has been widely investigated in recent years and has proven to be most promising in making C_{2+} products.[15] ZnO nanorods were already researched in our group and revealed a Faradaic Efficiency of 45% towards CO.[44]

4.2.1. Catalyst characterization

SEM-EDX

To determine the shape and size of the synthesized particles, SEM images were made. The SEM results in Figure 16 show the Cu_2O nanocubes and ZnO nanorods after synthesis. The cubes (on the left) are monodisperse, but look a bit fluffy and lack sharp edges. The larger cubes seem to have a hole in the middle. This suggests that eight cubes have agglomerated to form one bigger cube. On the right side of Figure 16, the obtained nanorods after hydrothermal synthesis are depicted. The nanorods are well-defined, however, particles of two different sizes are visible: larger particles of circa 5 µm in length and smaller particles of roughly 1 µm.

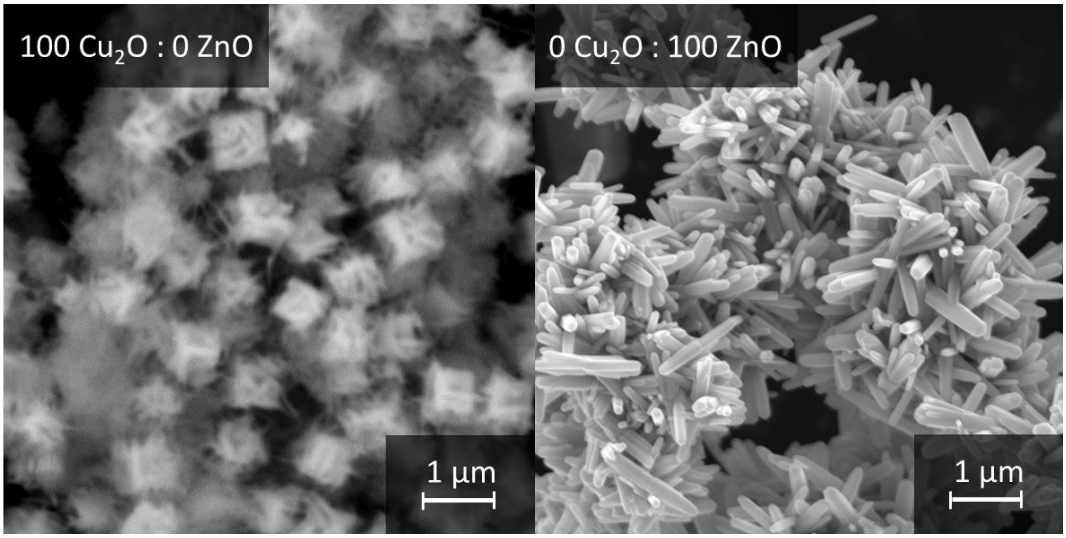

***Figure 16**. SEM images of the Cu_2O nanocubes (left) and ZnO nanorods (right) after synthesis.*

Four ratios of Cu_2O:ZnO ink will be compared in this research: 100 Cu_2O : 0 ZnO, 90 Cu_2O : 10 ZnO, 75 Cu_2O : 25 ZnO and 0 Cu_2O : 100 ZnO. The SEM images below show the electrodes after drop casting with the four separate inks before catalysis, see Figure 17. In the top row, the electrodes with monometallic copper (left) and monometallic zinc (right) are depicted. As expected, nanocubes and nanorods covered by binder are observed. The particles themselves did not change in shape or size. We do see some particles that are embedded deeper and some that lie at the surface of the electrode.

In the bottom row, we see the electrodes with mixed Cu_2O and ZnO nanoparticles in two different ratios (90 Cu_2O : 10 ZnO on the left and 75 Cu_2O : 25 ZnO on the right). The left image shows platelets have formed of roughly the same size the Cu_2O cubes would be. Also, big lumps of agglomerated platelets are observed. We expect these platelets to be ZnO particles, since they are known to exist in platelet shape and these were also observed in the galvanic replaced electrodes (see section 4.1.4). The right image shows a cloud of Nafion binder, with a few cubes and rods (see appendix K for more images). The cubes and rods do not appear in close proximity, but this is difficult to say because some particles might be obscured by binder.

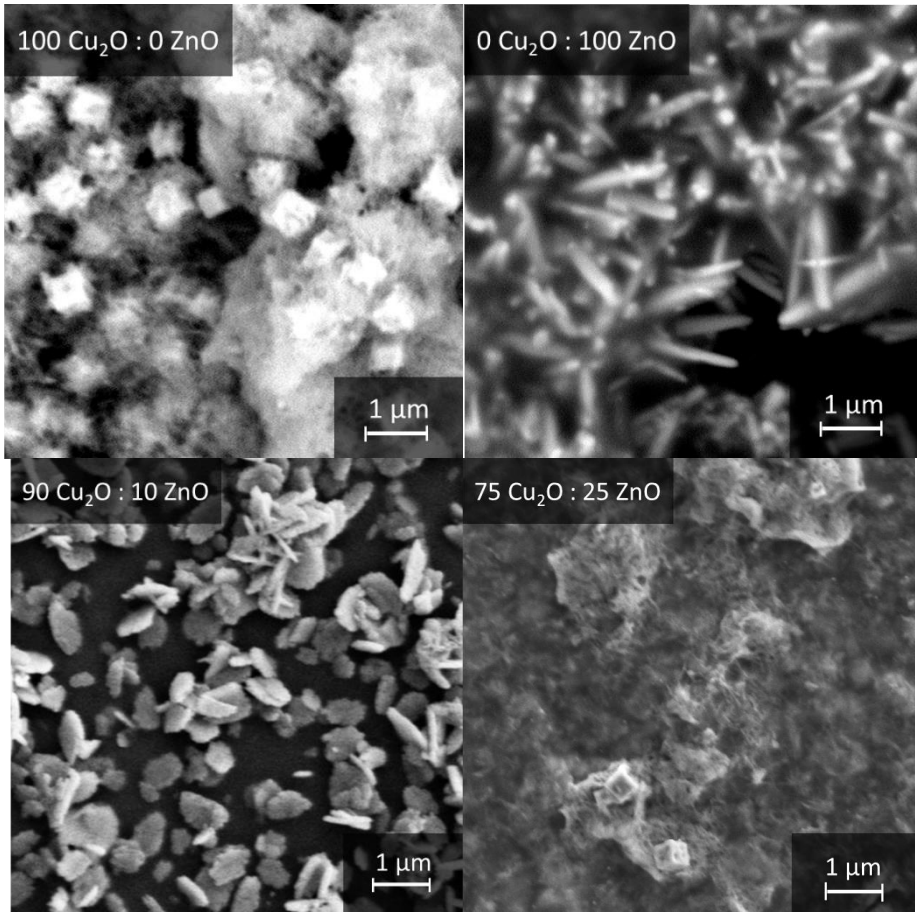

Figure 17. *SEM images from the drop casted electrodes before catalysis.*

X-Ray Diffraction

Before catalysis, the diffractograms of all electrodes depict peaks corresponding to ZnO, Cu_2O or glassy carbon (the broad peak around 50°), see Figure 18. Remarkably, different ratios of the [200] (at 50°) versus [111] (at 47°) of Cu_2O are observed for the three electrodes with Cu_2O, whilst the same batch of Cu_2O cubes is used. In the 90 Cu_2O : 10 ZnO sample, the [200] peak, indicating cubes, is absent or obscured by the peak of the glassy carbon. The low indication of the [200] site corresponds with the SEM images of the sample, in which no cubes were observed. The other samples with Cu_2O nanocubes drop casted do display this [200] peak at a 2θ of 50 degrees. These different ratios of the [200] versus [111] peak could be the result of preferential orientations of the particles with different Cu_2O:ZnO ratios.

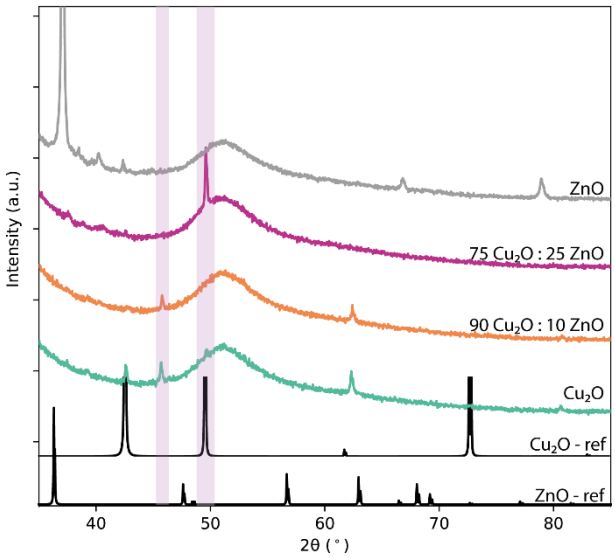

Figure 18. *The normalized diffractograms of the synthesized electrodes before catalysis.*

4.2.2. Activity

Catalytic performance was tested by operating chronoamperometry on five different potentials (-0.8, -0.9, -1.0, -1.1 and -1.2 V vs RHE) two or three times each. The resistance was measured beforehand and corrected for during each measurement.

Figure 19 shows the total current density during catalytic measurements for the four different electrodes. A few differences are discovered between the monometallic electrodes and the bimetallic electrodes. Firstly, the current density for the bimetallic electrodes reach slightly higher cathodic values than the monometallic electrodes (-8 mA/cm^2 versus -6 mA/cm^2). Secondly, the standard deviation of the current of all electrodes becomes higher at more cathodic potentials. Thirdly, the standard deviations are greater when zinc and copper are combined than for monometallic zinc or copper.

One factor of importance could be the iR shift in potential, which becomes greater at more cathodic currents and is significant because of the relatively high cell resistance of around 30 Ω. Another factor could be limitations of the transport of CO_2 to the electrode at high current densities due to the poor solubility of CO_2 in aqueous electrolytes.[15] However, this is especially important at current densities higher than 20 mA/cm^2. At a maximum current density of circa -8 mA/cm^2, we do not expect to observe these problems.[22] A third factor is the expected inconsistency of the synthesis method, more variables causes a greater inconsistency, thus creating a bimetallic system increases the possibility of deviations. A fourth and last factor of importance is the fact that copper and zinc combined might increase the activity by display of the CO spillover effect.

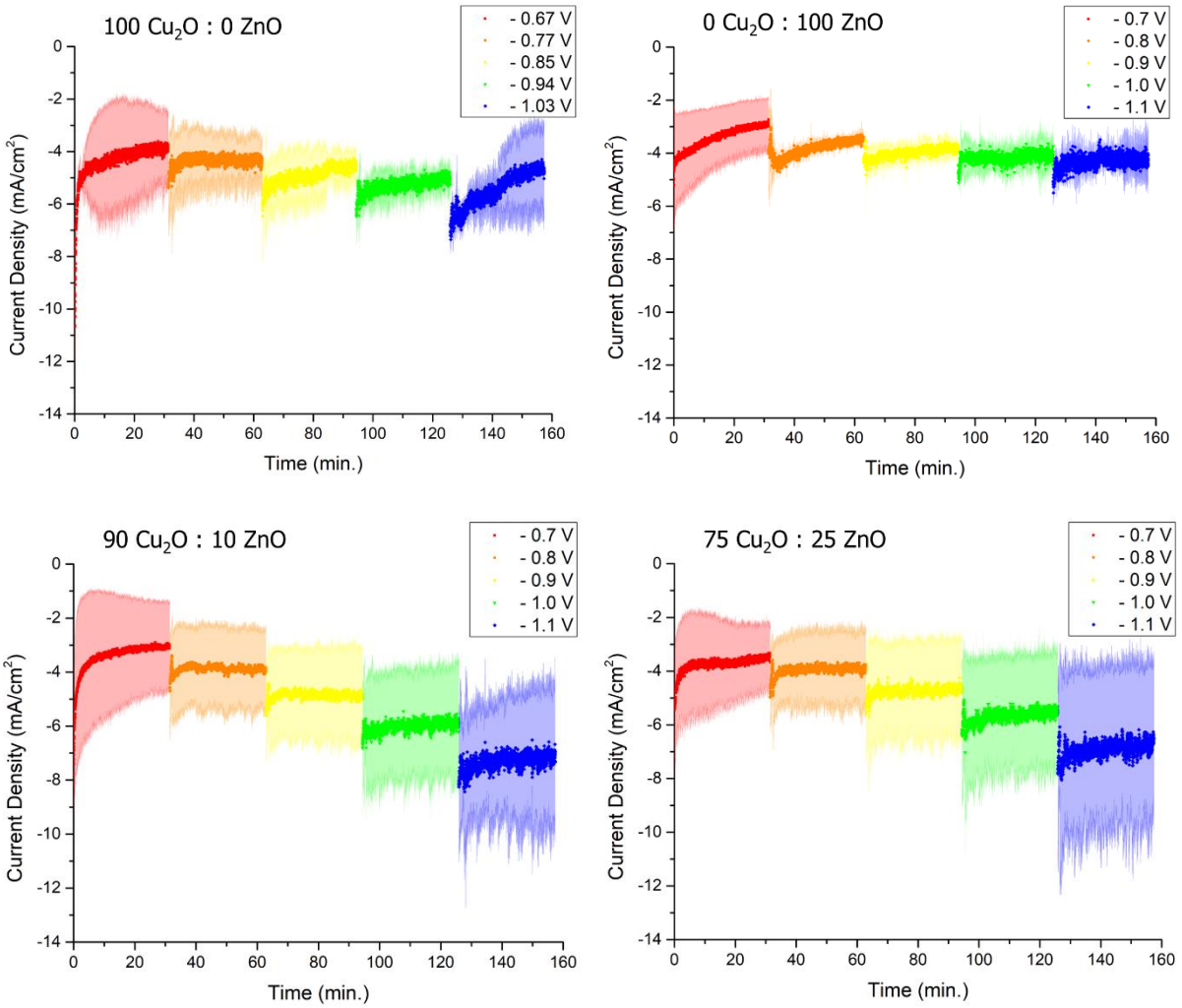

Figure 19. *The total current density in mA/cm^2 during catalytic measurements for the four different electrodes on five potentials vs RHE plotted against the time.*

4.2.3. Selectivity

To find the interesting elemental ratios for this study, multiple samples were made and tested for two hours at a fixed potential. The results are depicted in appendix G. No other C_{2+} products than C_2H_4 and EtOH were observed in significant amounts.

It is known that the CO_2RR selectivity is strongly potential dependent. Therefore, the catalytic performance was measured at five different potentials in the range of -0.8 V to -1.2 V and performed three times to verify the reproducibility. In Figure 20, the catalytic performance of the four electrodes is shown. As expected, the catalyst with 100% Cu_2O produces multiple products – hydrogen and carbon monoxide, hydrocarbons and alcohols. Since this research is mainly focusing on C_{2+} products, only ethylene and ethanol (the C_{2+} products observed) are depicted in the graphs. Graphs with all formed products can be found in appendix H. The catalyst with only ZnO forms exclusively hydrogen and carbon monoxide. Interestingly, the catalysts with mixed Cu_2O and ZnO particles also show formation of C_{2+} products, in contrast to the galvanic replaced samples discussed before.

A first note must be made about the significant amount of missing faradaic efficiency observed. A first reason for the missing electrons is the reduction of the catalyst metal oxides. To quantify this contribution, a calculation was executed to determine the maximum value in faradaic efficiency

originating from the reduction of Cu_2O and ZnO. This calculation proved that only 0.9% faradaic efficiency could originate from the reduction of Cu_2O and ZnO. The calculations are included in appendix I. Therefore, this contribution is negligible for our results. A second reason might be the oxidation of product to CO_2 and H_2O. Since products are observed in both catholyte and anolyte, it can be concluded that the anion exchange membrane is not selectively permeable. Therefore, we might oxidise products at the counter electrode. This might also explain the loss of products such as ethanol discussed below (section *shift from ethylene to ethanol formation*).

When the product distribution between the samples is compared, interesting differences can be observed. Copper is known to produce significant amounts of hydrogen, more than zinc. We can see this corresponds with our catalytic results for the electrodes of Cu_2O and ZnO for all potentials in the graph. Especially, at a potential range of -0.8 V to -1 V a high faradaic efficiency for hydrogen is observed for the Cu_2O electrode. The electrodes with mixed Cu_2O and ZnO show a higher faradaic efficiency for hydrogen than ZnO, but lower than Cu_2O.

When the CO production between the four samples is compared, it is obvious that the 100 Cu_2O : 0 ZnO electrode makes the least. The more zinc is added to the copper electrode, the higher the faradaic efficiency for CO is observed. Interestingly, when partial current densities for CO formation are compared, the electrode with 75 Cu_2O : 25 ZnO shows a higher CO formation than the electrode with only ZnO, see appendix H.

Ethylene and ethanol formation are mostly observed in the potential range of -1 V to -1.2 V, which corresponds values described in literature.[21] Ethylene formation increases with increasing potential for all electrodes including copper. More ethanol is formed when 10 or 25 percent zinc is present in the electrode, especially at moderate overpotentials around -1 V. This phenomenon is also discussed in the paper of Koper *et al*. for the cubes, where 100% Cu cubes produced 15% ethanol and 90% Cu with 10% Zn cubes produced approximately 20% ethanol.[15] The considerable formation of ethanol around -1 V for both mixed electrodes as compared to the 100% Cu_2O electrode is remarkable. Especially since the ethylene formation for the mixed electrodes is lower than for the 100% Cu_2O electrode. This suggests that the selectivity for the CO_2RR can be shifted towards the formation of ethanol by adding zinc to a copper catalyst.

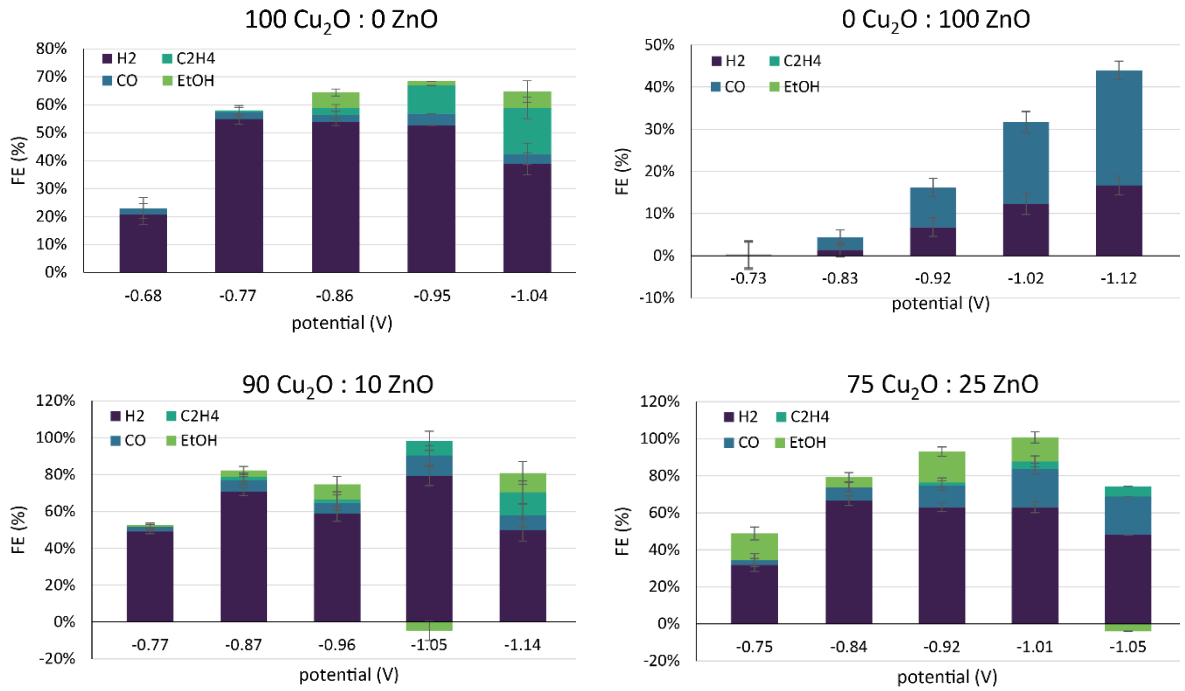

Figure 20. *Faradaic efficiency for hydrogen, carbon monoxide, ethylene and ethanol depicted for the four different samples (100* Cu_2O *: 0 ZnO, 0* Cu_2O *: 100 ZnO, 90* Cu_2O *: 10 ZnO and 75* Cu_2O *: 25 ZnO), measured at five different potentials, all depicted vs RHE.*

Shift from ethylene to ethanol formation

Figure 21 highlights the ethylene and ethanol selectivity of the different electrodes at three different potentials. From this figure, it can be concluded that the faradaic efficiency for ethylene increases with increasing cathodic potential and increasing copper content. The 100 Cu_2O : 0 ZnO electrode produces more ethylene at the least cathodic potential than the 90 Cu_2O : 10 ZnO electrode, which in turn produces more than the 75 Cu_2O : 25 ZnO electrode. This sequence applies to all three potentials displayed. Interestingly, this trend is reversed if we look at ethanol. The ethanol FE shows a maximum at -1.05 V for the 100 Cu_2O : 0 ZnO electrode. For the 90 Cu_2O : 10 ZnO electrode, the maximum FE is 8% at -0.94 V. The 75 Cu_2O : 25 ZnO shows even higher ethanol FE at this potential, 17%. This implies that the selectivity of the copper electrocatalyst shifts from ethylene to ethanol formation with the addition of zinc.

This shift from ethylene to ethanol formation has been recognized before in literature for Cu-Ag systems[18] and a hypothesis for the mechanism has been proposed by Ting et al.[17] With their Cu-Ag bimetallic system, the ethanol:ethylene ratio shifted from 0.4 in a monometallic copper electrocatalyst to 1.1 in the bimetallic catalyst. Ting et al. ascribe this shift to the abundant CO availability at Cu-Ag boundaries, facilitating the *CO diffusion and promoting the coupling of *CO and *CH_x species. This results in an increased formation of the *COCH species, intermediate in the reaction pathway for ethanol. Iyengar et al. describe similar results, but include the ratio to be even greater when octahedral copper particles are used. Recently, Dongare *et al.* showed similar results for a CuO-ZnO_x catalyst, increasing the ethanol production from 9% for monometallic copper to 22.3% in the bimetallic catalyst.[13]

The negative faradaic efficiency for ethanol observed at -1.05 V for the electrodes with zinc added can have multiple explanations. First of all, products are observed in the anolyte, which indicates an unselective permeable membrane for our products. If our counter electrode oxidizes the products to CO_2 and H_2O, a loss of products is observed. A second explanation could be the condensation of liquid products during catalysts, when gas is bubbled, or during storage in the NMR tube.

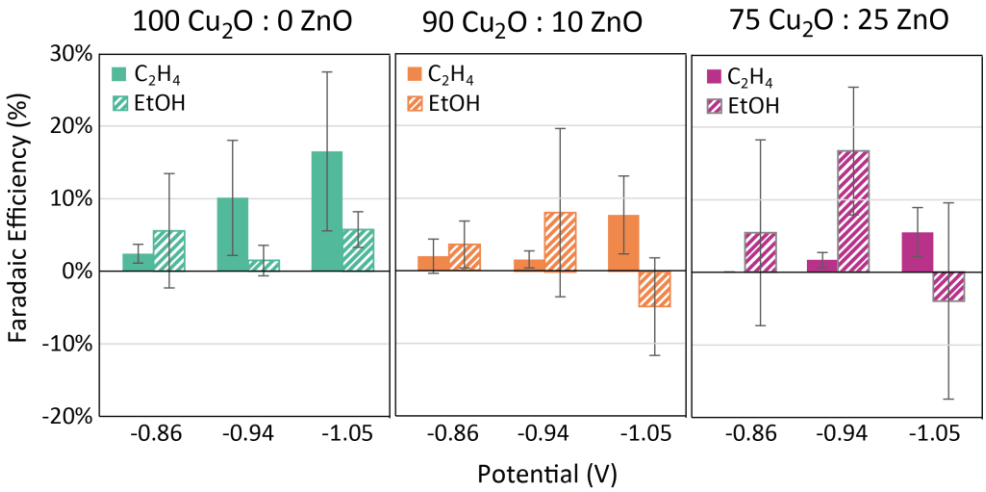

Figure 21. *The faradaic efficiency in % for ethylene (filled) and ethanol (stripes) plotted against the potential in V.*

4.2.4. Stability

SEM-EDX

To verify the stability of our catalyst during a measurement, SEM images were taken after catalysis, see Figure 22. All four electrocatalysts show a big change in morphology during the catalytic measurement, this restructuring is expected to be the result of a dissolution-redeposition mechanism, where Zn is oxidized to Zn^{2+} and redeposited on the electrode.[60,61] This is the result of zinc being unstable in water, see the Pourbaix diagram in section 2.2.1. In the electrode with only Cu_2O, dendrites have grown. We expect that fragmentation into smaller particles has taken place, followed by agglomeration to form these larger dendritic structures. This clustering is observed in literature, where it is ascribed to the high potential used during catalysis.[62] On the electrodes with mixed Cu_2O and ZnO particles, the particles have fragmented into many smaller particles. On the 0 Cu_2O : 100 ZnO electrode, an absence of particles is observed, which is confirmed by EDX (Appendix K).

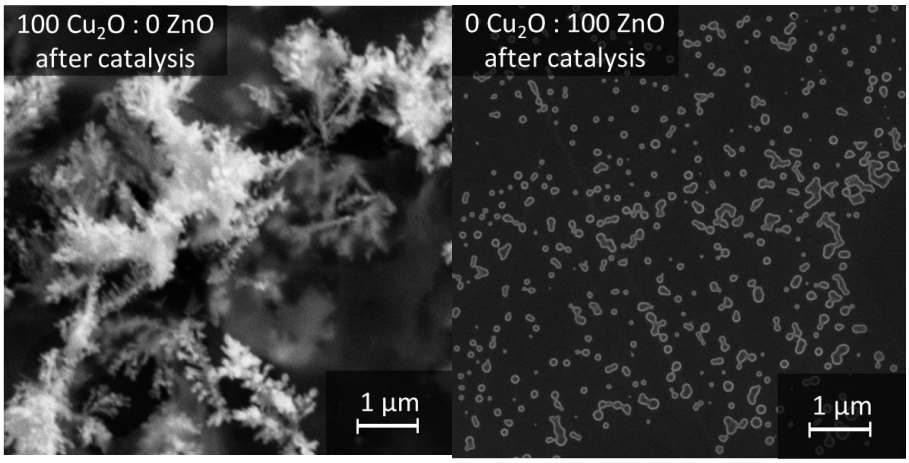

Figure 22. *SEM images from the drop casted electrodes after catalysis.*

The particles on the electrode with 90 Cu_2O : 10 ZnO after catalysis were too small for the EDX signal to be accurate, see Figure 23. For the electrode with 75 Cu_2O : 25 ZnO, a combination of larger particles in the micrometre range and smaller particles in the nanometre range are present. EDX confirms the bigger particles to be bimetallic copper/zinc and the smaller particles to be monometallic copper. No monometallic zinc particles are observed. We also see some big plates, which according to the EDX mapping contain Nafion binder with copper/zinc cubes inside, see appendix K.

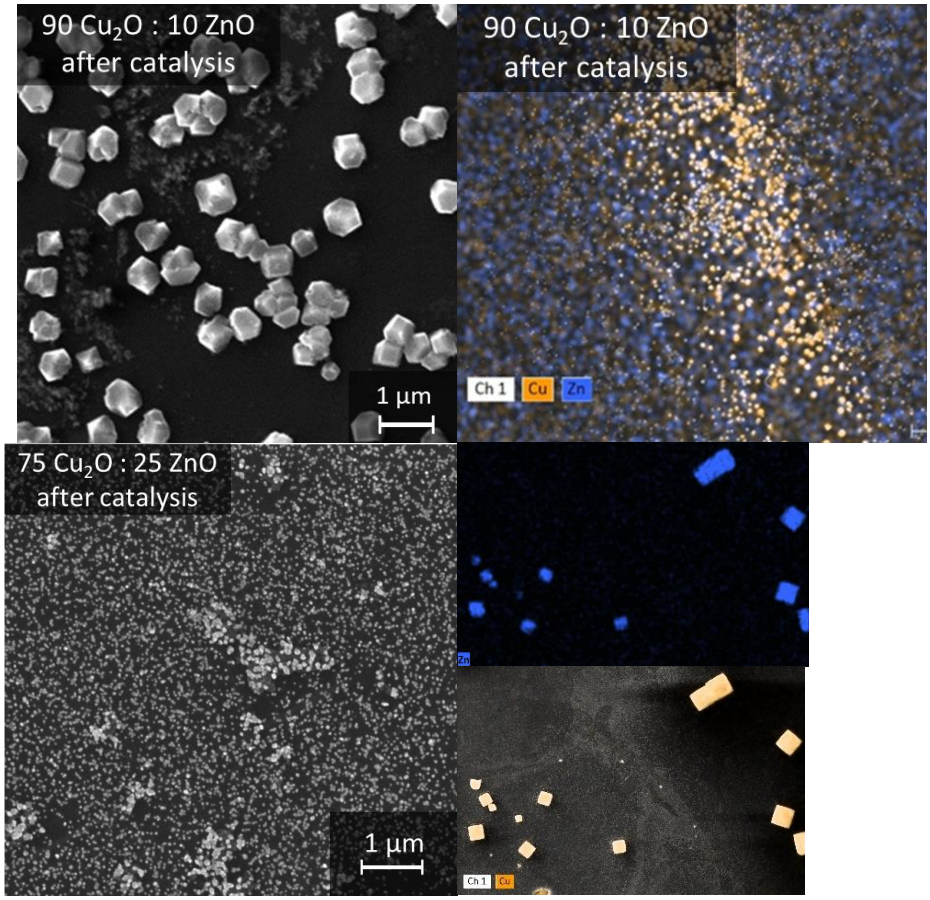

Figure 23. *SEM images from the drop casted electrodes with mixed Cu_2O and ZnO particles after catalysis (on the left) and SEM-EDX measurements with zinc and copper overlay (on the right).*

It appears that particles are lost under CO_2RR conditions, since all the SEM images show less particles than before catalysis. But looking at the activity and the total product formation that stay constant after two hours, it is unlikely that all zinc dissolved. According to research conducted by Loiudice *et al*., nanocubes are intrinsically more active than spheres, but smaller particles exhibit higher activity than bigger particles.[63] Therefore, we might lose activity in our catalysis by going from cubic shapes to spheres, but gain activity in going from relatively large to smaller particles. A second explanation could be that the particles are too small to see in SEM. It would be interesting to look at TEM images to get a better resolution. A third explanation is the detachment of Nafion binder, which extracts the copper and zinc particles. However, this does not explain why more zinc than copper is lost.

X-Ray Diffraction

The XRD after catalysis shows no peaks for the electrodes with only Cu_2O particles and only ZnO particles, see Figure 24. The two electrodes with mixed Cu_2O and ZnO particles do show peaks corresponding to ZnO. The 75 Cu_2O : 25 ZnO electrode shows peaks corresponding to both ZnO and Zn, which indicates that the ZnO is reduced during catalysis. The extent of which is difficult to ascertain due to possible reoxidation in air. The SEM-EDX results indicated bimetallic copper/zinc structures to be present, however, we did not observe these in the XRD patterns. Probably, the signal is obscured by the glassy carbon background signal. The 90 Cu_2O : 10 ZnO electrode shows new peaks after catalysis, at 40°, 45°, 55° and 58°, corresponding to carbonates and salts.

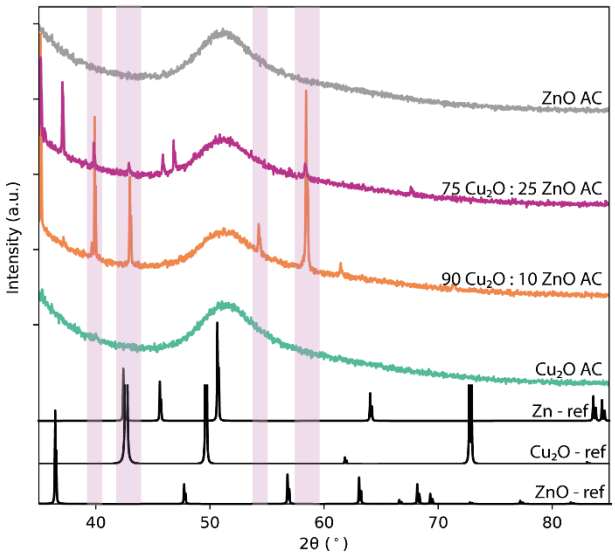

Figure 24. *The normalized diffractograms of the synthesized electrodes after catalysis.*

4.2.5. ICP results

Both the SEM-EDX and XRD results after catalysis suggest that we lose particles of our glassy carbon. This could either be during catalysis or during our washing treatment after catalysis, which helps us to remove some of the electrolyte salts formed on the electrode surface. Both electrolyte and wash water were measured with ICP for traces of zinc and/or copper. In the catholyte, large quantities of zinc and copper were observed (up to 42 and 29% of the starting quantities, respectively). This is peculiar because we would expect our activity to drop when losing particles and thus surface area. The washing water did not contain significant amounts of zinc and copper. This shows that we lose a significant amount of catalyst during catalysis.

4.2.6. Discussion/Summary drop casting

ZnO nanorods Cu_2O nanocubes were drop casted in different ratios and catalytically tested on -0.8, -0.9, -1.0, -1.1 and -1.1 V vs RHE for thirty minutes. The activity of the bimetallic electrodes was increased with circa 3 mA/cm^2 compared to the monometallic electrodes. The reproducibility of the bimetallic electrodes proved difficult, giving rise to great standard deviations in current density of circa 2 mA/cm^2. The mixed electrodes produced C_{2+} products during catalysis and a shift from ethylene to ethanol formation was observed when ZnO was added to a Cu_2O catalyst. This shift is described in literature for CuAg systems due to the CO spillover effect, where the abundance of CO in solution causes CO to bind to copper and react with *CH. The obtained *COCH is an intermediate for ethanol formation.

Both zinc and copper is altered in morphology during catalysis. In copper, dendrite formation is observed, which is a known morphology for copper structures. Zinc dissolves (is observed in the catholyte) and therefore decreases the stability of the catalyst.

5. Conclusions and Outlook

5.1. Conclusions

In order to overcome both the problem of emission of greenhouse gasses and the problem of the depletion of our energy source, alternative energy sources have been investigated. Since CO_2 is the most prominent greenhouse gas and an abundant carbon source, the reduction of this molecule into hydrocarbons and alcohols (C_{2+} products) would be a step forwards in closing the carbon cycle. A highly investigated method for this conversion is the electrochemical CO_2 reduction reaction (eCO_2RR), since it can be carried out in an electrochemical cell that operates at room temperature and in aqueous solution.[7] Hence, this is a sustainable reaction in case renewable electricity is used.

Copper is the only metal that can make C_{2+} products in significant amounts. However, the selectivity is still a big problem. There are multiple ways to improve this such as changing the morphology or using a second metal as promotor, the latter being used in this project. CO spillover effects can be observed if the second metal produces CO selectively, since CO is the main intermediate of the CO_2 reduction reaction. Thus, the addition of zinc to a copper catalyst is promising in showing an improved selectivity in the CO_2RR due to synergistic effects. Making this electrode an interesting candidate for a more selective, stable and active catalyst.

Galvanic replacement

Synthesising copper zinc electrodes via galvanic replacement was successfully executed, with multiple copper-zinc ratios as a result. With increasing copper content, the morphology of the zinc foil changed to pebble-like structures with increasing size. The X-ray diffractogram indicates that metallic copper structures have grown on top of the zinc foil, but copper has not infiltrated the hexagonal structure of zinc.

Activity measurements were performed on potentials between -0.8 and -1.0 V to investigate the performance of the electrodes during catalysis. All electrodes showed similar and stable current densities during the two hours of measuring. The product formation during this catalytic tests consisted of H_2 and CO, in different ratios. An optimum partial current density of CO was observed when 2.9 - 6.2 atomic% of copper was present. This optimum is most likely caused by a promoting and a deteriorating effect counteracting. The promoting effect is conceivably an increase in electrochemical surface area, resulting in additional CO production. However, since the electrochemical surface area is undetermined in this project, further research is necessary. A suggestion for the deteriorating effect is the addition of copper in the Zn/Cu epsilon phase, increasing hydrogen formation. More research is crucial to confirm this hypothesis.

Oxide derived particles

ZnO nanorods were synthesised via hydrothermal synthesis and Cu_2O nanocubes via the method described by Huang *et al*.[47] The ZnO particles were identical in shape but polydisperse, with particles of both 1 µm and 5 µm present. The Cu_2O nanocubes were monodisperse (circa 50 nm) but lack sharp edges. After drop casting with different Cu_2O:ZnO ratios, all particles were covered by Nafion binder.

The electrodes with different Cu_2O:ZnO ratios were catalytically tested on -0.8, -0.9, -1.0, -1.1 and -1.1 V vs RHE for thirty minutes. Both bimetallic electrodes had a higher activity than the monometallic electrodes with a maximum current density values of circa -8 mA/cm^2 versus -5 mA/cm^2, respectively. The reproducibility of the bimetallic electrodes proved difficult, giving rise to great standard deviations in current density of circa 2 mA/cm^2. The mixed electrodes produced C_{2+} products during catalysis and a shift from ethylene to ethanol formation was observed when ZnO was added to a Cu_2O catalyst. This

shift is described in literature for bimetallic systems due to the CO spillover effect, where the abundance of CO in solution causes CO to bind to copper and react with *CH. The obtained *COCH is an intermediate for ethanol formation.[18] Both zinc and copper is altered in morphology during catalysis. In copper, dendrite formation is observed, which is a known morphology for copper structures. Zinc is observed in the catholyte and therefore decreases the stability of the catalyst.

This research gives evidence for the tunability of the selectivity for the CO_2 reduction reaction (CO_2RR) by adding different amounts of zinc to a copper catalyst.

5.2. Outlook

Various investigations can be conducted as follow-up research for this project. First of all, it is difficult to keep the reaction conditions consistent over multiple measurements. Especially the galvanic replaced samples showed difficulties, since it was impossible to correct for the resistance in the cell, due to the set-up used. To be able to keep the potential stable over different samples, it is necessary to compensate for the resistance and measure it beforehand.

Furthermore, an optimum was observed in the current density for CO in galvanic replaced samples with an atomic% of copper between 2.9 and 6.2. To determine the promoting and deteriorating effect in this reaction, it would be interesting to synthesise the epsilon phase homogeneously and measure it in catalysis. This way, the product distribution in the CO_2RR for the Zn:Cu epsilon phase can be determined, giving knowledge on the effect it had on the reaction performed in this research.

Another unknown factor in this reaction is the electrochemical surface area. Therefore, it is uncertain if the effect seen in the production of CO is due to the increased Cu:Zn ratio or an altered electrochemical surface area. To establish the effect of the electrochemical surface area in this research, it is necessary to calculate the roughness effect value. When more knowledge is gained on these effects, it would be interesting to synthesise the optimum and perform catalysis on multiple potentials for longer time, to see the potential dependence and stability of the catalyst.

To gain more knowledge on the stability of the oxide-derived electrodes, TEM images could be made. These will give a better indication of the morphology of the remained particles after catalysis and EDX can help to obtain the composition, since TEM has a better resolution than the SEM images that were used in this research. Furthermore, other binders or a combination of different binders could be used to see if this helps in maintaining the particles. Multiple suggestions have been reported in literature about pre- and posttreatments, such as hot pressing methods, and variations in the ink formation, such as differences in solvents, ionomer, and additives.[64] Moreover, shorter measurements can be executed to gain knowledge on the change in morphology and dissolution of zinc over time.

To get a better look at the shift from ethylene to ethanol, different follow-up experiments can be executed. Firstly, a different morphology of the Cu_2O and ZnO particles can be catalytically tested, since the ethanol:ethylene ratio is described to be even higher for octahedral than for cubic particles in literature.[18] Moreover, it would be worth investigating the optimal Cu:Zn ratio to be used for tuning the selectivity of the CO_2RR towards ethanol. In the research of Iyengar et al. ratios of 2:3 Cu:Zn are used, while our maximal performance is at 75 Cu_2O : 25 ZnO. The addition of more ZnO might drive the ethanol formation even further. Another way to investigate a maximum is by testing the Cu_2O particles using CO or a CO/CO_2 mixture as a starting gas. By using CO as a starting gas, a potential threshold in the CO spillover effect can be found.

A challenge observed in this thesis in the production of ethanol is the diffusion of our products through the anion exchange membrane and anolyte, where it is oxidized to CO_2 and H_2O. Therefore, we lose products. Research with different membranes is necessary to look at the influence of this diffusion.

Performing the reaction in a flow cell will have multiple advantages. First of all, the flow cell is able to get to higher currents than an H-cell.[12] Secondly, it would prevent the oxidation of the products at the anodic side. Thirdly, the detachment of particles can be the result of bubble formation in the H-cell, this will be prevented in a flow cell.

6. Acknowledgements

With the end of my master thesis I would like to thank everyone who helped me during my time in the MCC group. A special thanks to Matt Peerlings for his daily supervision, the nice motivational talks and all the help on and around the lab. As a perfectionist I very much learnt that chaos brings creativity. I really liked working with you, even though I am already replaced by a new master student 😉. Then, I would like to thank dr. Peter Ngene for providing this project by being my first examiner and giving useful input during our meetings. I would like to thank prof. dr. Petra de Jongh for being my second examiner and for saying “gogogo” during my go-nogo.

I would like to thank Maaike van Ittersum for measuring ICP for me, answering my burning questions while Matt was away and listening to me while practising my go-nogo presentation. Some more people I would like to thank are Francesco Mattarozi and Valerio Gulino and all electrostudents: Karen van den Akker, Alexander Flick, Alex Klaver, Bo van Schie, Naud van de Ven, even Floris and Thom for the last two weeks and especially Mei Ju for warmly welcoming me into your territory. The biweekly meeting of the electrocatalysis group was a nice, especially after we introduced the cookies tradition. The last people I would like to thank are Dennie Wezendonk, Hans Meeldijk, Jan Willem de Rijk, Remco and Léon Witteman for help with the XRD, SEM, potentiostat, autoclave and NMR.

7. References

[1] V. Smil, *Energy Transitions: Global and National Perspectives*, Praeger, An Imprint Of ABC-CLIO, LLC, Santa Barbara, California, **2017**.
[2] Y. Jia, F. Li, K. Fan, L. Sun, *Advanced Powder Materials* **2022**, *1*, 100012.
[3] D. T. Whipple, P. J. A. Kenis, *J. Phys. Chem. Lett.* **2010**, *1*, 3451–3458.
[4] M. Lenzen, *Energies* **2010**, *3*, 462–591.
[5] M. North, R. Pasquale, C. Young, *Green Chem.* **2010**, *12*, 1514.
[6] M. Watanabe, M. Shibata, A. Kato, M. Azuma, T. Sakata, *J. Electrochem. Soc.* **1991**, *138*, 3382–3389.
[7] S. Garg, M. Li, A. Z. Weber, L. Ge, L. Li, V. Rudolph, G. Wang, T. E. Rufford, *J. Mater. Chem. A* **2020**, *8*, 1511–1544.
[8] J. Albo, M. Alvarez-Guerra, P. Castaño, A. Irabien, *Green Chem.* **2015**, *17*, 2304–2324.
[9] A. Bagger, W. Ju, A. S. Varela, P. Strasser, J. Rossmeisl, *ACS Catal.* **2019**, *9*, 7894–7899.
[10] K. P. Kuhl, E. R. Cave, D. N. Abram, T. F. Jaramillo, *Energy Environ. Sci.* **2012**, *5*, 7050.
[11] E. I. Solomon, P. M. Jones, J. A. May, *Chem. Rev.* **1993**, *93*, 2623–2644.
[12] S. Wang, T. Kou, S. E. Baker, E. B. Duoss, Y. Li, *Materials Today Nano* **2020**, *12*, 100096.
[13] S. Dongare, N. Singh, H. Bhunia, P. K. Bajpai, *Electrochimica Acta* **2021**, *392*, 138988.
[14] K. Jiang, Y. Huang, G. Zeng, F. M. Toma, W. A. Goddard, A. T. Bell, *ACS Energy Lett.* **2020**, *5*, 1206–1214.
[15] A. H. M. da Silva, S. J. Raaijman, C. S. Santana, J. M. Assaf, J. F. Gomes, M. T. M. Koper, *Journal of Electroanalytical Chemistry* **2021**, *880*, 114750.
[16] Z. Chang, S. Huo, W. Zhang, J. Fang, H. Wang, *J. Phys. Chem. C* **2017**, *121*, 11368–11379.
[17] L. R. L. Ting, O. Piqué, S. Y. Lim, M. Tanhaei, F. Calle-Vallejo, B. S. Yeo, *ACS Catal.* **2020**, *10*, 4059–4069.
[18] P. Iyengar, M. J. Kolb, J. R. Pankhurst, F. Calle-Vallejo, R. Buonsanti, *ACS Catal.* **2021**, *11*, 4456–4463.
[19] C.-Y. Liu, C.-C. Sung, *Journal of Power Sources* **2012**, *220*, 348–353.
[20] D. Ren, J. Fong, B. S. Yeo, *Nat Commun* **2018**, *9*, 925.
[21] S. Nitopi, E. Bertheussen, S. B. Scott, X. Liu, A. K. Engstfeld, S. Horch, B. Seger, I. E. L. Stephens, K. Chan, C. Hahn, J. K. Nørskov, T. F. Jaramillo, I. Chorkendorff, *Chem. Rev.* **2019**, *119*, 7610–7672.
[22] D. Ren, B. S.-H. Ang, B. S. Yeo, *ACS Catal.* **2016**, *6*, 8239–8247.
[23] A. Bagger, W. Ju, A. S. Varela, P. Strasser, J. Rossmeisl, *ChemPhysChem* **2017**, *18*, 3266–3273.
[24] C. Xiao, J. Zhang, *ACS Nano* **2021**, *15*, 7975–8000.
[25] J. Huang, M. Mensi, E. Oveisi, V. Mantella, R. Buonsanti, *J. Am. Chem. Soc.* **2019**, *141*, 2490–2499.
[26] D. L. T. Nguyen, M. S. Jee, D. H. Won, H. Jung, H.-S. Oh, B. K. Min, Y. J. Hwang, *ACS Sustainable Chem. Eng.* **2017**, *5*, 11377–11386.
[27] D. Ren, Y. Deng, A. D. Handoko, C. S. Chen, S. Malkhandi, B. S. Yeo, *ACS Catal.* **2015**, *5*, 2814–2821.
[28] J. He, N. J. J. Johnson, A. Huang, C. P. Berlinguette, *ChemSusChem* **2018**, *11*, 48–57.
[29] C. W. Li, J. Ciston, M. W. Kanan, *Nature* **2014**, *508*, 504–507.
[30] E. L. Clark, C. Hahn, T. F. Jaramillo, A. T. Bell, *J. Am. Chem. Soc.* **2017**, *139*, 15848–15857.
[31] Y. Ma, J. Yu, M. Sun, B. Chen, X. Zhou, C. Ye, Z. Guan, W. Guo, G. Wang, S. Lu, D. Xia, Y. Wang, Z. He, L. Zheng, Q. Yun, L. Wang, J. Zhou, P. Lu, J. Yin, Y. Zhao, Z. Luo, L. Zhai, L. Liao, Z. Zhu, R. Ye, Y. Chen, Y. Lu, S. Xi, B. Huang, C. Lee, Z. Fan, *Advanced Materials* **2022**, *34*, 2110607.
[32] Y. Zheng, J. Zhang, Z. Ma, G. Zhang, H. Zhang, X. Fu, Y. Ma, F. Liu, M. Liu, H. Huang, *Small* **2022**, *18*, 2201695.
[33] F. Jia, X. Yu, L. Zhang, *Journal of Power Sources* **2014**, *252*, 85–89.
[34] M. R. Broadley, P. J. White, J. P. Hammond, I. Zelko, A. Lux, *New Phytologist* **2007**, *173*, 677–702.
[35] U. Mizutani, in *Book Series on Complex Metallic Alloys*, WORLD SCIENTIFIC, **2010**, pp. 323–399.
[36] S. Ikeda, A. Hattori, K. Ito, H. Noda, *Electrochemistry* **1999**, *67*, 27–33.

[37] S. Zhen, G. Zhang, D. Cheng, H. Gao, L. Li, X. Lin, Z. Ding, Z. Zhao, J. Gong, *Angew Chem Int Ed* **2022**, *61*, e202201913.
[38] Z. Wang, X. Jiao, D. Chen, C. Li, M. Zhang, *Catalysts* **2020**, *10*, 1127.
[39] M. T. Weller, T. Overton, J. Rourke, F. A. Armstrong, *Inorganic Chemistry*, Oxford University Press, Oxford, United Kingdom, **2018**.
[40] C. Kim, F. Dionigi, V. Beermann, X. Wang, T. Möller, P. Strasser, *Advanced Materials* **2019**, *31*, 1805617.
[41] M. Ahlers, *Progress in Materials Science* **1986**, *30*, 135–186.
[42] P. De Luna, R. Quintero-Bermudez, C.-T. Dinh, M. B. Ross, O. S. Bushuyev, P. Todorović, T. Regier, S. O. Kelley, P. Yang, E. H. Sargent, *Nat Catal* **2018**, *1*, 103–110.
[43] Y. Hori, H. Wakebe, T. Tsukamoto, O. Koga, *Surface Science* **1995**, *335*, 258–263.
[44] K. Han, P. Ngene, P. Jongh, *ChemCatChem* **2021**, *13*, 1998–2004.
[45] P. Grosse, A. Yoon, C. Rettenmaier, A. Herzog, S. W. Chee, B. Roldan Cuenya, *Nat Commun* **2021**, *12*, 6736.
[46] R. M. Arán-Ais, R. Rizo, P. Grosse, G. Algara-Siller, K. Dembélé, M. Plodinec, T. Lunkenbein, S. W. Chee, B. R. Cuenya, *Nat Commun* **2020**, *11*, 3489.
[47] W.-C. Huang, L.-M. Lyu, Y.-C. Yang, M. H. Huang, *J. Am. Chem. Soc.* **2012**, *134*, 1261–1267.
[48] G. O. Mallory, American Electroplaters and Surface Finishers Society, Eds. , *Electroless Plating: Fundamentals and Applications*, American Electroplaters And Surface Finishers Soc, Orlando, Fla, **1990**.
[49] A. G. M. da Silva, T. S. Rodrigues, S. J. Haigh, P. H. C. Camargo, *Chem. Commun.* **2017**, *53*, 7135–7148.
[50] C. Kong, S. Sun, J. Zhang, H. Zhao, X. Song, Z. Yang, *CrystEngComm* **2012**, *14*, 5737.
[51] T. Ahmad, *MSEIJ* **2018**, *2*, DOI 10.15406/mseij.2018.02.00040.
[52] T. B. Massalski, H. W. King, *Acta Metallurgica* **1962**, *10*, 1171–1181.
[53] C. Brito, C. A. Siqueira, J. E. Spinelli, A. Garcia, *Materials Letters* **2012**, *80*, 106–109.
[54] J. Jiang, H. Huang, J. Niu, Z. Jin, M. Dargusch, G. Yuan, *Scripta Materialia* **2021**, *200*, 113907.
[55] D. Ma, Y. Li, S. C. Ng, H. Jones, *Acta Materialia* **2000**, *48*, 419–431.
[56] C. G. Morales-Guio, E. R. Cave, S. A. Nitopi, J. T. Feaster, L. Wang, K. P. Kuhl, A. Jackson, N. C. Johnson, D. N. Abram, T. Hatsukade, C. Hahn, T. F. Jaramillo, *Nat Catal* **2018**, *1*, 764–771.
[57] D. Raciti, M. Mao, J. H. Park, C. Wang, *J. Electrochem. Soc.* **2018**, *165*, F799–F804.
[58] B. Qin, H. Wang, F. Peng, H. Yu, Y. Cao, *Journal of CO2 Utilization* **2017**, *21*, 219–223.
[59] A. Kaliyaraj Selva Kumar, Y. Zhang, D. Li, R. G. Compton, *Electrochemistry Communications* **2020**, *121*, 106867.
[60] J. Vavra, T. Shen, D. Stoian, V. Tileli, R. Buonsanti, *Angewandte Chemie* **2021**, *133*, 1367–1374.
[61] S. B. Varandili, D. Stoian, J. Vavra, K. Rossi, J. R. Pankhurst, Y. T. Guntern, N. López, R. Buonsanti, *Chem. Sci.* **2021**, *12*, 14484–14493.
[62] J. Huang, N. Hörmann, E. Oveisi, A. Loiudice, G. L. De Gregorio, O. Andreussi, N. Marzari, R. Buonsanti, *Nat Commun* **2018**, *9*, 3117.
[63] A. Loiudice, P. Lobaccaro, E. A. Kamali, T. Thao, B. H. Huang, J. W. Ager, R. Buonsanti, *Angew. Chem. Int. Ed.* **2016**, *55*, 5789–5792.
[64] T. Jaster, S. Albers, A. Leonhard, M.-A. Kräenbring, H. Lohmann, B. Zeidler-Fandrich, F. Özcan, D. Segets, U.-P. Apfel, *J. Phys. Energy* **2023**, *5*, 024001.

8. Appendix

Galvanic Replacement

A Photos of the synthesised electrodes

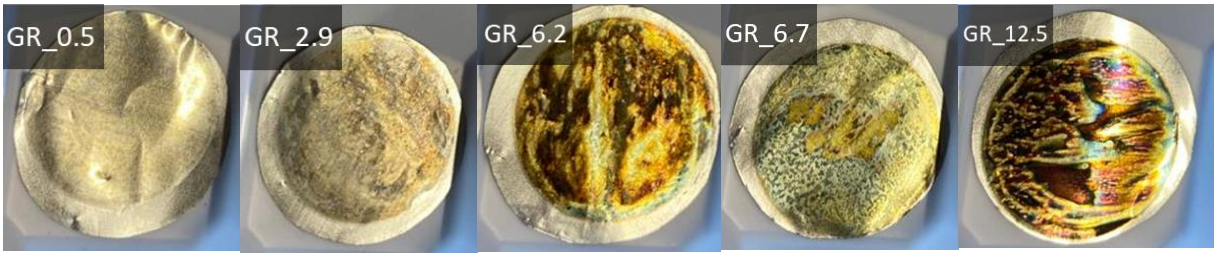

B SEM-EDX

The following weight percentage of different elements was obtained via EDX:

Naam	$Cu(NO_3)_2$ (mM)	Zinc (%)	Copper (%)	Oxygen (%)
GR_0.5	1	96.2	0.5	3.3
GR_2.9	2.5	82.9	2.9	14.3
GR_6.2	7.5	84.9	6.2	8.9
GR_6.7	5	84.6	6.7	8.7
GR_12.5	10	75.5	12.5	12.1

The SEM images of extra samples after catalysis. In every sample, the copper and zinc is mixed, except for GR03. For GR_2.9, we can see the copper is concentrated on the small particles. GR03 was made with 100 mM copper nitrate solution, but the copper content was not measured.

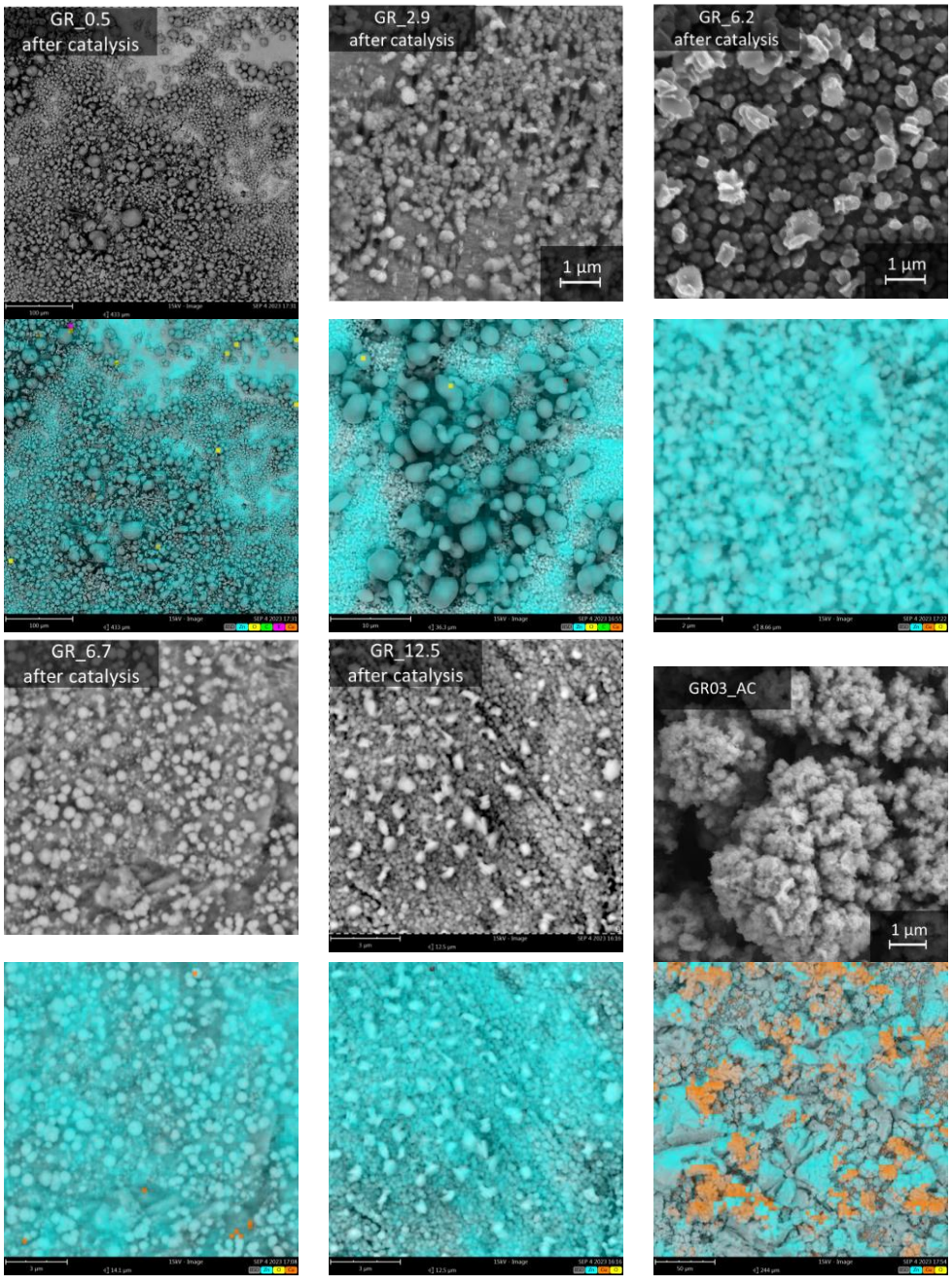

C Calculated fit by Origin

Model	Lorentz		
Equation	y = y0 + (2*A/PI)*(w/(4*(x-xc)^2 + w^2))		
Reduced Chi-Sqr	0.85526		
Adj. R-Square	0.82023		
		Value	Standard Error
iCO	y0	0.56251	0.6877
iCO	xc	6.00371	1.13071
iCO	w	13.70553	4.11167
iCO	A	115.26273	39.08431
iCO	H	5.35394	0.91013

D Double Layer Capacitance

Linear Sweep Voltammetry was performed on the zinc foil and copper foil in a wide potential range, to find the best potential range for double layer capacitance, see the figures below. The best range seems to be between 0 and 0.2 V vs RHE, however, at this potential the zinc dissolves. At the rest of the potentials, no region was observed where both zinc and copper showed no reactions.

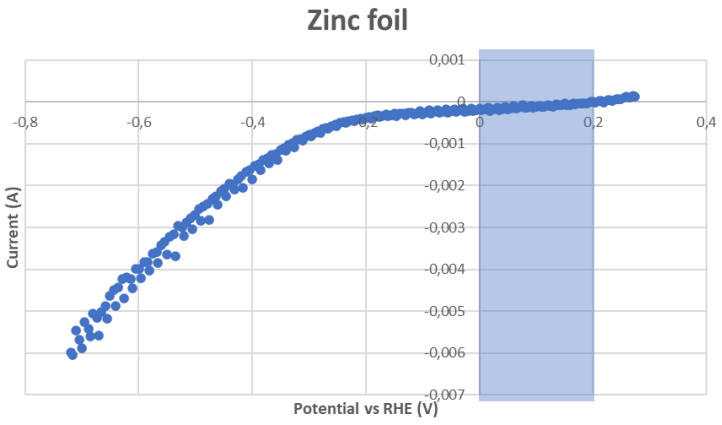

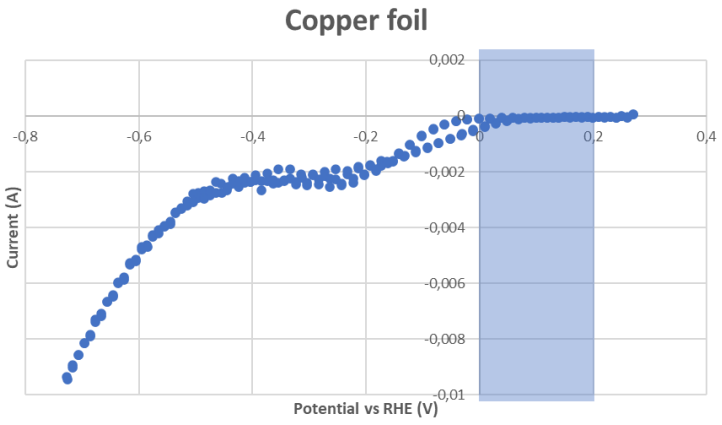

Oxide-derived Cu2O-ZnO based electrodes

E Sample ratios

A list of all sample names with different Cu_2O:ZnO ratios is given.

Name	Cu2O atomic %	µL Cu2O ink	ZnO atomic %	µL ZnO ink
8A	100	250	0	0
8B	90	225	25	30
8C	75	187.5	10	62.5
8D	0	0	100	250

F Photos of the synthesised electrodes

100 Cu_2O : 0 ZnO | 90 Cu_2O : 10 ZnO | 75 Cu_2O : 25 ZnO | 0 Cu_2O : 100 ZnO

G fixed potential study

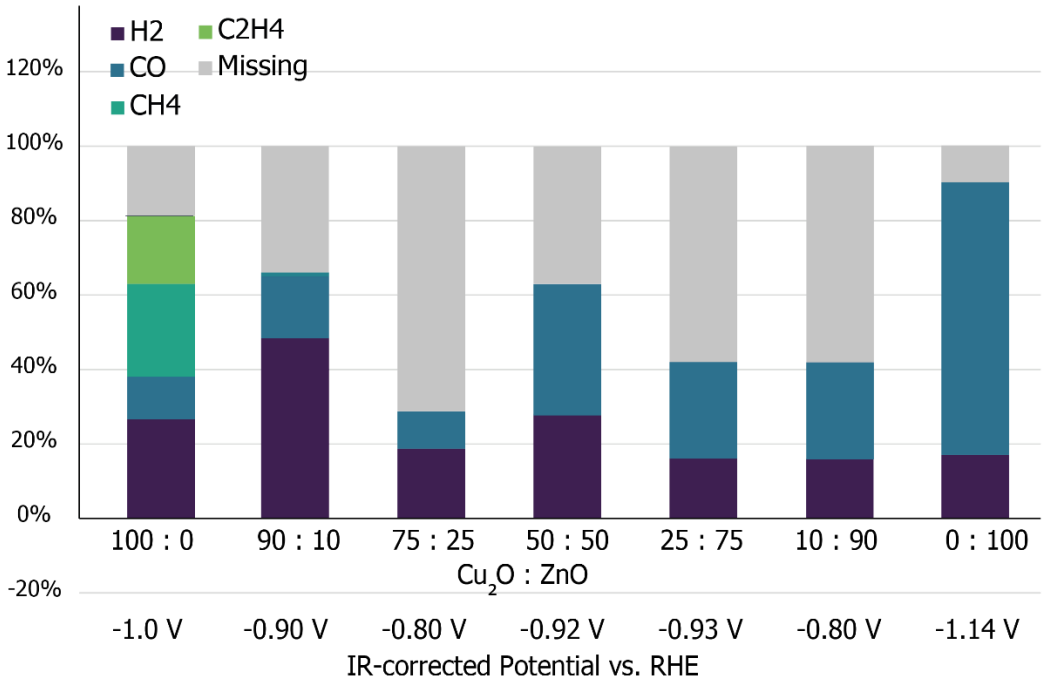

The figure below shows the current density of the different Cu_2O : ZnO electrodes over time, measured on a fixed potential (see the figure above for the potential per sample). The electrode with only ZnO shows the highest current density and therefore the least activity. The Cu_2O electrode has a slightly

increased activity. Interestingly, the electrodes with mixed Cu_2O and ZnO all show an increased activity compared to the electrodes with only one metal.

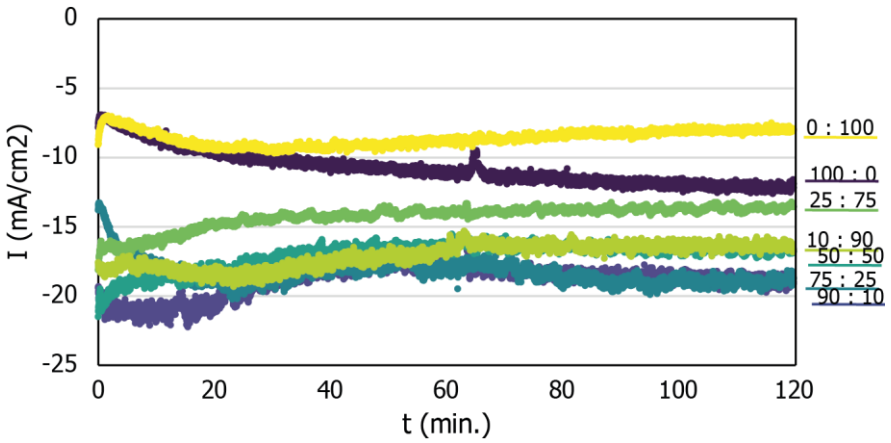

H Product distribution oxide-derived particles

The figures below show the faradaic efficiency for the four different electrodes.

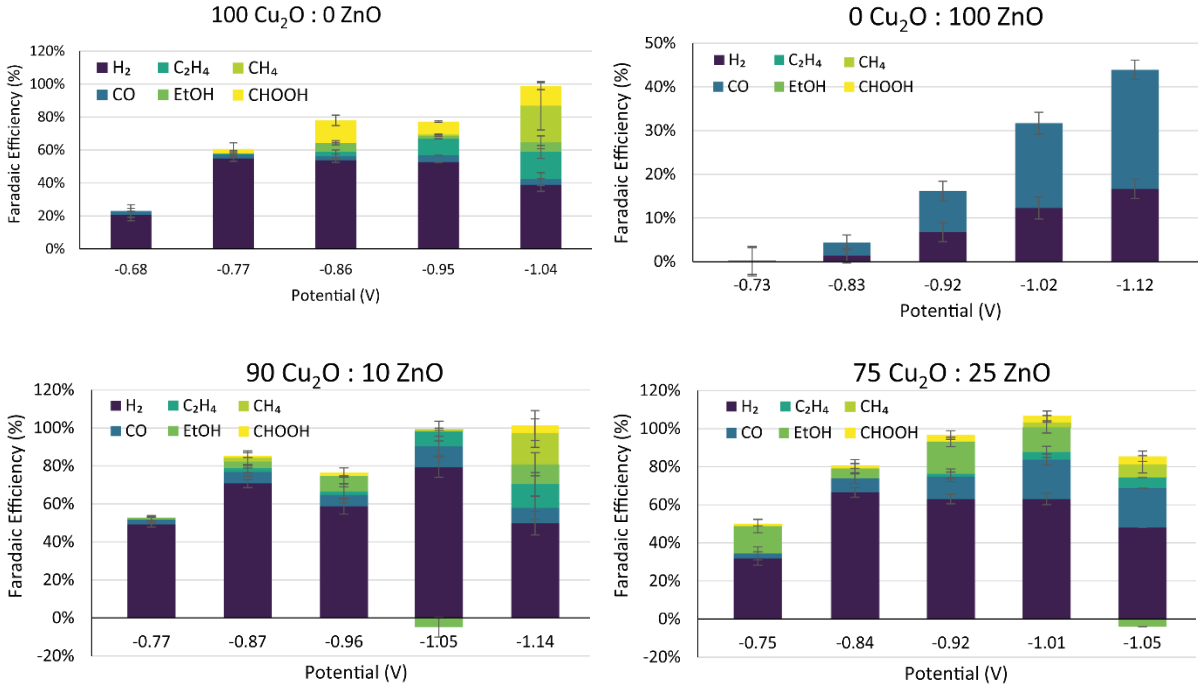

Figure 14. *Faradaic efficiency for hydrogen, carbon monoxide, ethylene and ethanol depicted for the four different samples (100* Cu_2O *: 0 ZnO, 0* Cu_2O *: 100 ZnO, 90* Cu_2O *: 10 ZnO and 75* Cu_2O *: 25 ZnO), measured at five different potentials, all depicted vs RHE.*

The figure below shows the partial current density used for producing a certain product by the four different electrodes.

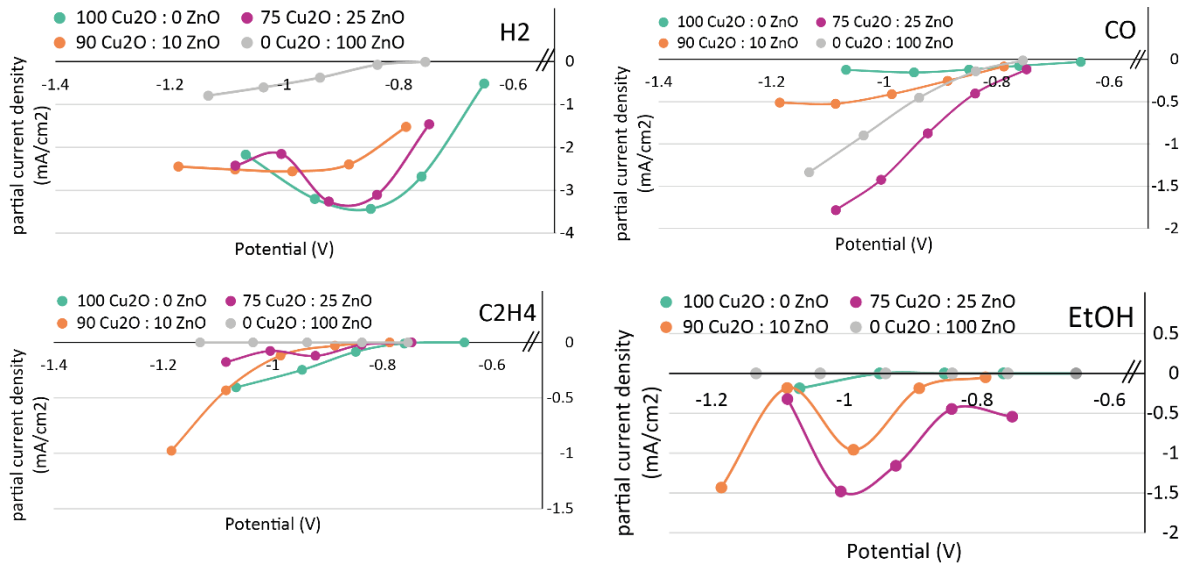

Figure 15. *The partial current density in mA used for producing a certain product from the CO_2RR (H_2, CO, C_2H_4 and EtOH, respectively) plotted against the potential in V.*

I Calculations missing FE

2 electrons are used in the reduction of one ZnO molecule.
In sample 7A (10 Cu2O : 90 ZnO), there was 0.05025 mg ZnO, corresponding to $6.1*10^{-7}$ mol ZnO.

$$96485\frac{C}{mol} * 2\left(\frac{e^-}{mol}\right) * 6.1 * 10^{-7}\ mol\ ZnO = 0.1177117\ C$$

$$partial\ current = \frac{0.1177117\ C}{7200\ s} = 1.63488 * 10^{-5}\ C/s$$

The total current measured was 0.018316 C/s

$$FE = \frac{partial\ current}{total\ current} = \frac{1.63488 * 10^{-5}}{0.018316} = 0.9\%$$

K EDX results oxide-derived Cu2O-ZnO based electrodes

Extra SEM images of 75 Cu_2O : 25 ZnO

The SEM images below show nanorods (on the left image) as well as nanocubes (on the right image) to be present in the 75 Cu_2O : 25 ZnO sample.

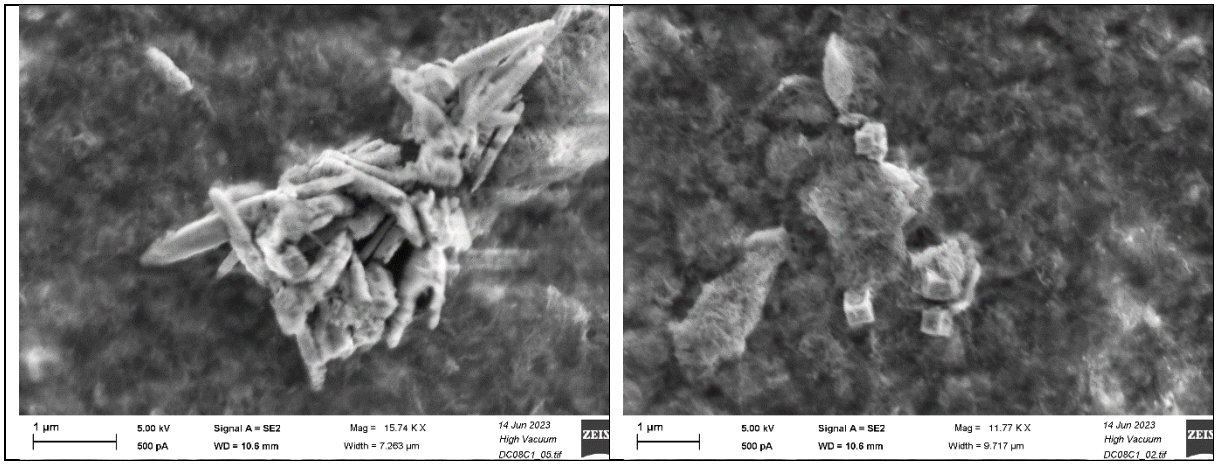

Nafion plate formation

As can be seen in the figures below, Nafion plates have formed during catalysis. The left image is an overview and the right image shows a zoomed in plate, where the cubes can be observed.

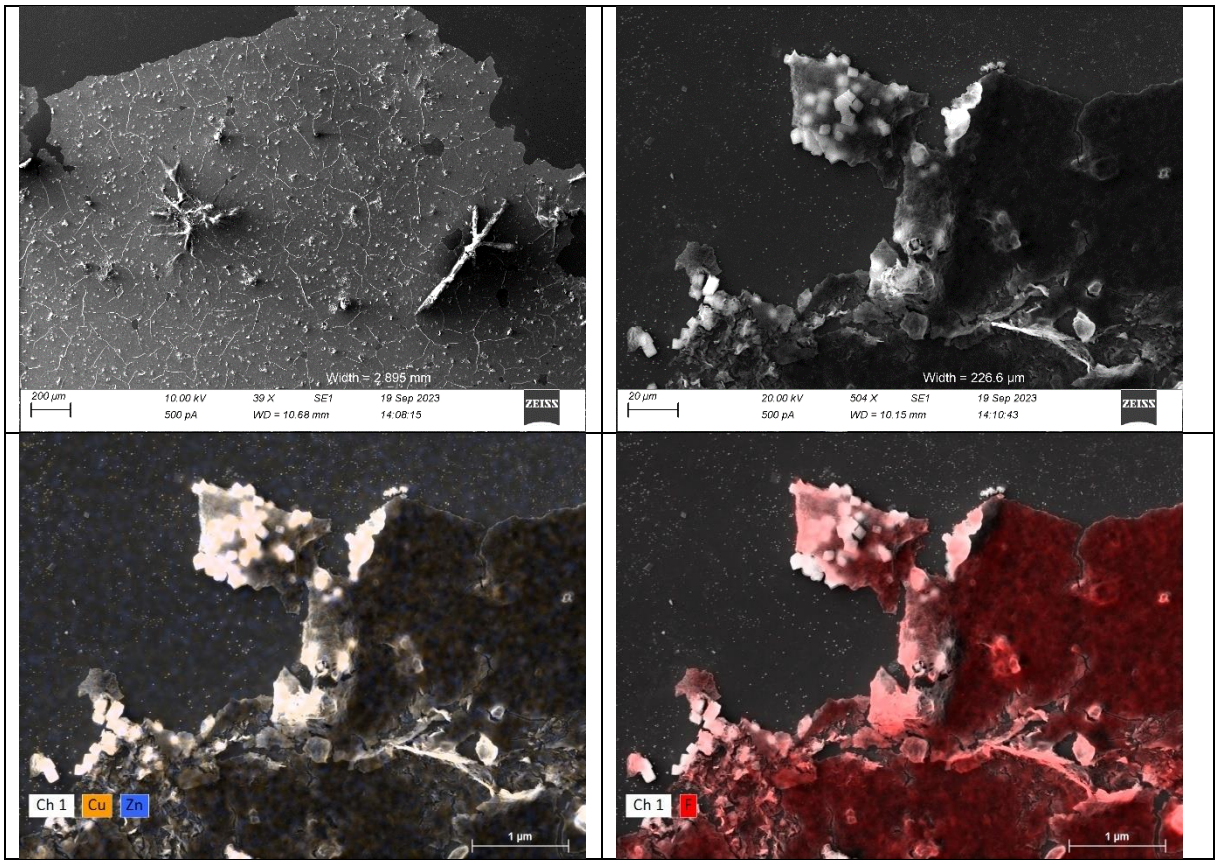

90 Cu2O : 10 ZnO electrode after catalysis

No zinc is observed in the SEM-EDX calculations after catalysis.

Element	At. No.	Netto	Mass [%]	Mass Norm. [%]	Atom [%]	abs. error [%] (1 sigma)	rel. error [%] (1 sigma)
Carbon	6	1142039	80,31	80,31	87,16	3,69	4,60
Oxygen	8	48484	13,16	13,16	10,72	0,71	5,37
Potassium	19	301871	6,03	6,03	2,01	0,10	1,70
Copper	29	5882	0,49	0,49	0,10	0,02	3,31
Zinc	30	104	0,01	0,01	0,00	0,01	75,92
Fluorine	9	0	0,00	0,00	0,00	0,00	5,13
		Sum	**100,00**	**100,00**	**100,00**		

ZnO electrode after catalysis

As can be seen in the figure below, the mass % for copper and zinc is negligible low in the 0 Cu_2O : 100 ZnO electrode after catalysis. The only elements measured are carbon, oxygen and potassium.

SPU0

Element	At. No.	Netto	Mass [%]	Mass Norm. [%]	Atom [%]	abs. error [%] (1 sigma)	rel. error [%] (1 sigma)
Carbon	6	1056776	77,81	77,81	84,96	3,62	4,66
Oxygen	8	62695	15,99	15,99	13,11	0,86	5,36
Potassium	19	250211	5,06	5,06	1,70	0,09	1,73
Copper	29	7900	0,65	0,65	0,13	0,02	2,87
Zinc	30	4753	0,47	0,47	0,09	0,02	3,74
Fluorine	9	86	0,01	0,01	0,01	0,01	90,83
		Sum	**100,00**	**100,00**	**100,00**		

L Particle ink measurements:

SEM images were made of the nanoparticle inks after different sonicating times. As we can see, the best distribution of the particles is after 30 minutes of sonicating.

Cu_2O ink:

0 min 10 min 20 min 30 min

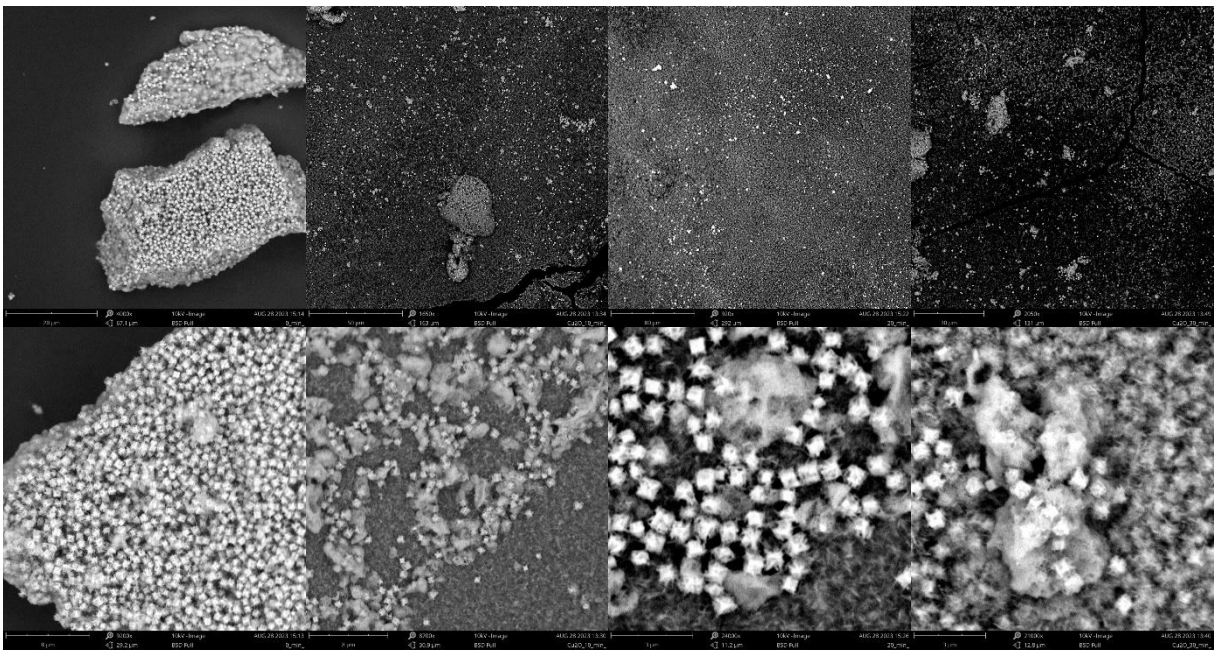

ZnO ink:

0 min 10 min 30 min